

# Enceladus Plume Density Modeling and Reconstruction for Cassini Attitude Control System

Siamak Sarani<sup>1</sup>

*Jet Propulsion Laboratory, California Institute of Technology*

In 2005, Cassini detected jets composed mostly of water, spouting from a set of nearly parallel rifts in the crust of Enceladus, an icy moon of Saturn. During an Enceladus flyby, either reaction wheels or attitude control thrusters on the Cassini spacecraft are used to overcome the external torque imparted on Cassini due to Enceladus plume or jets, as well as to slew the spacecraft in order to meet the pointing needs of the on-board science instruments. If the estimated imparted torque is larger than it can be controlled by the reaction wheel control system, thrusters are used to control the spacecraft. Having an engineering model that can predict and simulate the external torque imparted on Cassini spacecraft due to the plume density during all projected low-altitude Enceladus flybys is important. Equally important is being able to reconstruct the plume density after each flyby in order to calibrate the model. This paper describes an engineering model of the Enceladus plume density, as a function of the flyby altitude, developed for the Cassini Attitude and Articulation Control Subsystem, and novel methodologies that use guidance, navigation, and control data to estimate the external torque imparted on the spacecraft due to the Enceladus plume and jets. The plume density is determined accordingly. The methodologies described have already been used to reconstruct the plume density for three low-altitude Enceladus flybys of Cassini in 2008 and will continue to be used on all remaining low-altitude Enceladus flybys in Cassini's extended missions.

## Nomenclature

$a$	= X-axis tri-axial of Enceladus body, m
$A_{Proj}$	= spacecraft projected area, m <sup>2</sup>
$b$	= Y-axis tri-axial of Enceladus body, m
$c$	= Z-axis tri-axial of Enceladus body, m
$c_1, c_2, c_3$	= product of two cosines [see Eq. 31]
$C$	= a general factor [see Eq. 27]
$C_{Coef}$	= array of coefficient factors used for adjusting density [see Eq. 20]
$C_D$	= drag coefficient
$CM_x, CM_y, CM_z$	= X, Y, and Z coordinates of the spacecraft center of mass, m
$C_{J2000}^{Enc}$	= a transformation matrix from EME-2000 inertial frame to the Enceladus' body-fixed frame
$C_{RWA}^{SC}$	= a transformation matrix from reaction wheel frame to spacecraft's fixed frame
$d$	= number of days past 12:00 noon of 1/1/2000 epoch
$d_{Depth}$	= the depth of the plume cone apex below the surface of Enceladus, m
$d_{ES}$	= Enceladus-Saturn distance, km
$d_{ES,mean}$	= semi-major axis of the Enceladus' orbit around Saturn, km
$d_{QS}$	= distance from the plume center of activity to spacecraft's center of mass, m
$d_{Range}$	= distance between spacecraft's c.m. and Enceladus' c.m., m
$D_S$	= day of year for the start time of plume density model simulation, days
$\hat{e}_x, \hat{e}_y, \hat{e}_z$	= spacecraft body unit vectors in EME-2000 frame
$erf(\bullet)$	= error function ( $erf(x) = \frac{2}{\sqrt{\pi}} \int_0^x e^{-t^2} dt$ )
$F_0$	= steady-state thrust magnitude, N
$h$	= Enceladus flyby altitude, km
$h_0$	= array of altitudes used for adjusting the density model [see Eq. 20], km
$h_1$	= a general term [see Eq. 25], km
$h_{Thresh}$	= altitude threshold beyond which plume density is assumed to be constant, km
$H_d$	= depletion length scale which makes the total gas constant of the plume finite, km
$\vec{H}_{RWA}$	= total angular momentum vector of the three reaction wheels in body frames, Nms
$H_S$	= hours for the start time of plume density model simulation, hr

<sup>1</sup> Senior Member of Technical Staff, Guidance and Control Section, Jet Propulsion Laboratory, Mail Stop 230-104, 4800 Oak Grove Drive, Pasadena, California 91109-8099, USA. [Siamak.Sarani@jpl.nasa.gov](mailto:Siamak.Sarani@jpl.nasa.gov)

$H_{Plume,Fit}^Z$	= the smoothed angular momentum about spacecraft's Z-Axis due to plume torque, Nms
$H_{\psi}$	= angular width of plume, deg
$i$	= general subscript
$I$	= spacecraft's inertia tensor, $\text{kgm}^2$
$I_{min}$	= minimum moment of inertia of spacecraft, $\text{kgm}^2$
$I_{max}$	= maximum moment of inertia of spacecraft, $\text{kgm}^2$
$I_{res}$	= residual impulse associated with a single thruster pulse, Ns
$I_{xx}, I_{yy}, I_{zz}$	= principal moments of inertia, $\text{kgm}^2$
$k$	= numerical coefficient
$k_{JP}$	= the jet-to-plume ratio factor
$K$	= a general factor [see Eq. 25]
$M_S$	= minutes for the start time of plume density model simulation, min
$\bar{Q}$	= ascending node
$\vec{r}_{CM}$	= position vector for the spacecraft's center of mass relative to the origin of the spacecraft coordinate frame, m
$\vec{r}_{CP}$	= position vector for the spacecraft's center of pressure relative to the origin of the spacecraft coordinate frame, m
$\vec{r}_{J2000}$	= spacecraft position vector in J2000 frame, km
$r_{Jet}$	= radius of the cylinder associated with a jet
$R_0$	= distance from spacecraft's center of mass to center of Enceladus, km
$\hat{R}_0$	= unit vector along the vector connecting the spacecraft's center of mass to the center of Enceladus represented in the EME-2000 frame
$R_E$	= radius of Enceladus, km
$R_i$	= Rotation matrix about the $i^{\text{th}}$ axis
$S$	= molecular speed ratio
$S_1, S_2, S_3, S_4$	= set of angles, $^{\circ}$
$S_S$	= seconds for the start time of plume density model simulation, s
$t$	= time, s
$t_{ECA}$	= time of closest approach for Enceladus flyby, s
$t_R$	= rise-time constant, s
$t_T$	= tail-off time constant, s
$T$	= evaluation time given as an interval since the standard epoch ( $J2000$ ) in Julian centuries of 36525 days each
$T_{MLI}$	= spacecraft's multi-layer insulation skin temperature, K
$\vec{T}_{GG}$	= gravity-gradient torque imparted by Enceladus on Cassini, Nm
$\vec{T}_{Mag}$	= magnetic torque imparted on spacecraft due to Saturn/Enceladus magnetic fields, Nm
$\vec{T}_{Plume}$	= drag torque imparted on spacecraft due to plume and jets, Nm
$\vec{T}_{RTG}$	= torque imparted on the spacecraft due to radioisotope thermoelectric generator (RTG) thermal radiation, Nm
$\vec{T}_{RWA}$	= reaction torque imparted on spacecraft by three reaction wheels, Nm
$\vec{T}_{Sol}$	= solar radiation torque imparted on spacecraft, Nm
$\vec{T}_{Thruster}$	= torque imparted on spacecraft due to thruster firings, Nm
$T_{\infty}$	= Enceladus plume temperature, K
$\vec{T}_{\epsilon}$	= vector sum of external torques imparted on spacecraft but not accounted for in $\vec{T}_{Thruster}$ , $\vec{T}_{RWA}$ , and $\vec{T}_{Plume}$ , Nm
$\hat{u}_{PS}$	= unit vector along the vector connecting the plume cone apex to spacecraft's center of mass

$\hat{u}_Q$	= unit vector along the vector connecting Enceladus' center to the plume center of activity
$\hat{u}_{QS}$	= unit vector along the vector connecting the plume center of activity to spacecraft's center of mass
$\hat{u}_{SC}$	= unit vector along the vector connecting the Enceladus' center to spacecraft's center of mass
$\hat{u}_V$	= unit vector of spacecraft velocity as expressed in a spacecraft body frame
$V$	= magnitude of the body-fixed spacecraft velocity, m/s
$V_h$	= particle velocity component perpendicular to Enceladus' surface, m/s
$V_{th}$	= thermal velocity, m/s
$w$	= plume radius on surface, km
$W$	= prime meridian angular position from the line of nodes, rad
$x_1, x_2, x_3, x_4, x_5, x_6$	= components of the coefficient vector for angular momentum fitting function
$\vec{X}$	= coefficient vector for accumulated angular momentum fitting function
$X, Y, Z$	= spacecraft body axes
$\hat{X}_{Enc}, \hat{Y}_{Enc}, \hat{Z}_{Enc}$	= Enceladus body-fixed axes
$Y_S$	= year for the start time of plume density model simulation
$\hat{Z}_{J2000}$	= Z-axis of EME-2000 inertial frame
$\alpha_0$	= right ascension of Enceladus north pole of rotation, rad
$\beta$	= angle between the unit vectors $\hat{u}_{PS}$ and $\hat{u}_Q$ , °
$\beta_m$	= array of plume half cone angles, °
$\gamma$	= angle between the unit vectors $\hat{u}_{QS}$ and $\hat{u}_Q$ , °
$\delta_0$	= declination of Enceladus north pole of rotation, rad
$\Delta$	= commanded thruster Pulse width (s)
$\Delta_{ES}$	= distance margin, km
$\varepsilon$	= array of adjusting terms for altitude exponent [see Eq. 20]
$\vec{\zeta}$	= vector sum of the torques due to all possibly existing thruster leaks and all other un-modeled torques, Nm
$\theta$	= longitude, °
$\theta_{SS}$	= longitude of sub-satellite trajectory, °
$\theta_x, \theta_y, \theta_z$	= direction cosine angles determined from the dot product of $\hat{R}_0$ with spacecraft body axes in EME-2000 frame, $\hat{e}_x, \hat{e}_y, \hat{e}_z$ , respectively, °
$\lambda$	= distance from Enceladus' center to the center of plume activity, km
$\mu_{Enceladus}$	= gravitational parameter of Enceladus, $\text{km}^3/\text{s}^2$
$\rho$	= Enceladus plume density, $\text{kg}/\text{m}^3$
$\rho_0$	= plume density at the surface of Enceladus, $\text{kg}/\text{m}^3$
$\rho_{Res}$	= residual background density, $\text{kg}/\text{m}^3$
$\sigma$	= standard deviation
$\tau$	= a dummy variable representing time, s
$\tau_{max}^{GG}$	= worst-case gravity gradient torque, Nm
$\tau_x^{GG}, \tau_y^{GG}, \tau_z^{GG}$	= per-axis gravity gradient torque, Nm
$\varphi$	= latitude, °
$\varphi_{SS}$	= latitude of sub-satellite trajectory, °
$\psi$	= angular distance from the plume center, °
$\vec{\omega}$	= spacecraft's angular rate vector, rad/s
$\dot{\vec{\omega}}$	= spacecraft's angular acceleration vector, $\text{rad}/\text{s}^2$

## Cassini: 12 Years and Still Going Strong

The Cassini spacecraft (Fig. 1) is by far the largest and most sophisticated space vehicle ever built and sent by mankind to explore an outer planet of the Solar System. Managed by the Jet Propulsion Laboratory (JPL), a division of the California Institute of Technology in Pasadena, this amazing mission is an international cooperation involving the NASA, the European Space Agency (ESA), the Italian Space Agency, and several industrial and academic partners.<sup>1</sup> The Cassini spacecraft was launched on October 15, 1997 and after an interplanetary cruise of almost seven years, it arrived at Saturn on July 1, 2004. About six months after the completion of the Saturn orbit insertion, the Huygens probe, built by the ESA, was successfully released in December of the same year. Now after 12 years, Cassini is still going strong. It proceeds to conduct further scientific investigations of Saturn and its rings, magnetosphere, Titan, and icy moons especially the mysterious Enceladus. This successful mission has already completed its 4-year prime mission and is more than half way through its 2-year Equinox extended mission. After the completion of the Equinox mission around September 2010, Cassini will likely start its seven-year Solstice mission.<sup>1</sup>

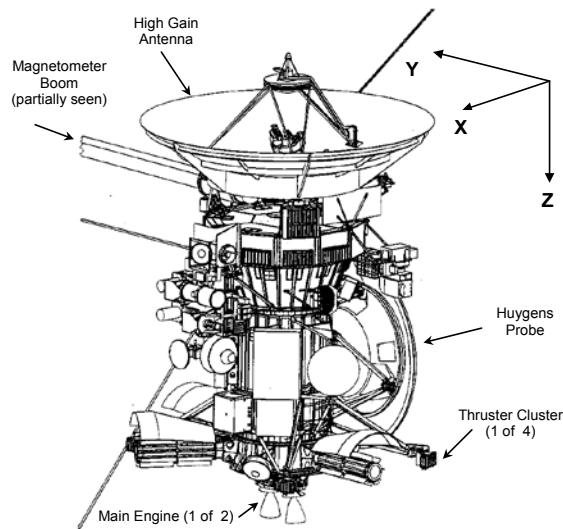


**Fig. 1 Cassini spacecraft with attached Huygens probe.**

Cassini's Attitude and Articulation Control System (AACS) estimates and controls the spacecraft attitude. It responds to ground-commanded pointing goals for the spacecraft's science instrument and communication antennas with respect to targets of interest. The AACS also executes ground-commanded spacecraft velocity changes. In order to maintain a stable attitude during the course of Cassini mission, two distinct control systems are used: the attitude controller using the Reaction Control System (RCS) thrusters, and the attitude controller using the reaction wheels.<sup>2</sup> An overview of the design and flight performance of the Cassini AACS is described in Reference 2.

Since 2005, the Cassini spacecraft has performed a few flybys of Enceladus. Some of these flybys have been at low altitudes, as low as 25 km. Enceladus is a remarkably active body having water jets that spout from a set of cracks on the moon's surface near its south polar region. Jets appear to emanate from four prominent rifts, called the Tiger stripes, which appear to be warmer than the surrounding terrain. During an Enceladus flyby, either attitude control thrusters or the reaction wheels are used to overcome the external torque imparted on Cassini due to Enceladus plume, and to turn the spacecraft for science observations. If the imparted torque is larger than the control authority of the reaction wheel system, the RCS thrusters will be used to control the spacecraft during the Enceladus flyby. This paper describes an engineering model of the Enceladus plume density and a methodology to estimate the external torque imparted on Cassini spacecraft due to the Enceladus plume and jets using the guidance, navigation, and control data. The plume density is determined accordingly.

## The Enigmatic Enceladus

Enceladus has sparked great excitement among scientists since the Cassini's discovery of the geyser activities on its surface. Enceladus (Fig. 2), an inner icy moon of Saturn, is only about 500 km in diameter.<sup>3</sup> Its disk area is not much bigger than the Great Britain. More accurately, as modeled by Cassini Navigation Team, Enceladus is in a shape of an ellipsoid with tri-axial X, Y, and Z dimensions of  $256.6 \pm 0.5$  km,  $251.4 \pm 0.2$  km, and  $248.3 \pm 0.2$  km, respectively.<sup>4</sup> Enceladus was discovered by William Herschel in 1789. It orbits Saturn between the moons Mimas and Tethys once every 32.88 Earth hours (1.37 days). Its average orbit distance from Saturn is about 238,020 km with orbit eccentricity of 0.0047 and with approximately  $0^\circ$  orbital inclination relative to ecliptic.<sup>4,5</sup> During the orbit around Saturn, the Enceladus-Saturn distance grows to 239.18 thousand kilometers at the apoapsis and drops to 236.89 thousand kilometers at the periapsis, and the difference between these two extremes is 2297.4 km.<sup>4,5</sup> The prime meridian of Enceladus (the X-axis of Enceladus-centric frame) lines up with the Enceladus-Saturn direction during both the apoapsis and periapsis. The gravitational parameter of Enceladus is  $7.21108 \text{ km}^3/\text{s}^2$ . Its average surface temperature is  $-200^\circ\text{C}$  (73 K).<sup>6</sup>

Enceladus is an amazingly active body with large, internally generated thermal anomaly.<sup>6,7,8</sup> Scientists have always been intrigued by Enceladus, even before Cassini-Huygens mission to Saturn. In July 2005, the scientific instruments onboard Cassini made a remarkable discovery that Enceladus is actively venting both plume and icy, dusty particles from relatively hot regions near its south pole.<sup>7,8,9</sup> This was puzzling to scientists because Enceladus is too small and too cold for such activity.<sup>6,10</sup> In that same year, Cassini also detected that the active jets emanate from a set of nearly parallel cracks or rifts in the crust near Enceladus' south pole<sup>7,8,9</sup>, nicknamed the "tiger stripes." The tiger stripes<sup>3</sup> (Figs. 2 and 3) are located within an area of high heat flux and run for about 130 km across the moon's southern polar region, from  $65^\circ$  south towards the south pole, and are approximately 2 km wide.<sup>7,8,9</sup>

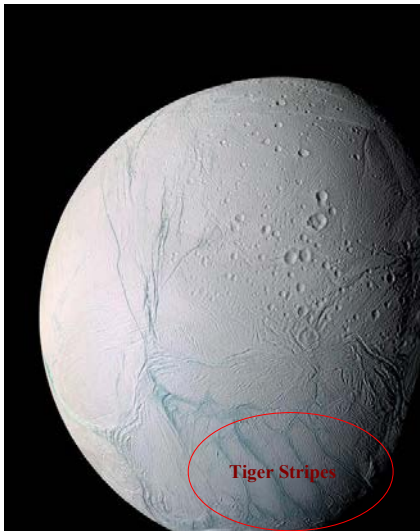


**Fig. 2 The Enceladus.** Courtesy of NASA JPL, Cassini Outreach.<sup>3</sup>

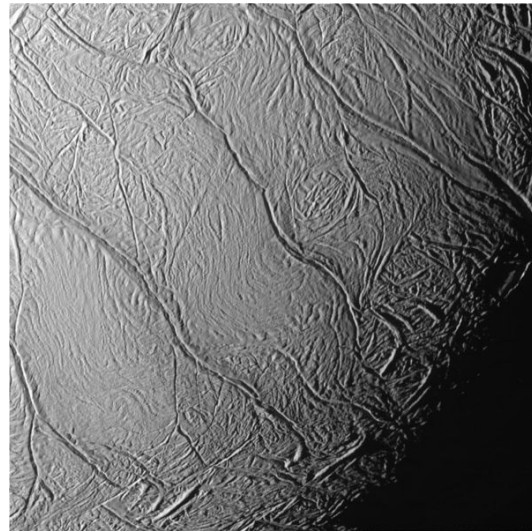


**Fig. 3 Tiger Stripes.** Courtesy of NASA JPL, Cassini Outreach.<sup>3</sup>

Jets appear to erupt from four prominent tiger stripe fissures (Figs. 4 and 5) dubbed Alexandria (A), Cairo (C), Baghdad (B), and Damascus (D).<sup>7,8</sup> The stronger sources of jets are on Baghdad and Damascus, and the sources on Baghdad seem to be the strongest of all. Interestingly, all the jets from each crack lie in a nearly vertical plane.<sup>8</sup> Again in 2005, Cassini's Composite Infrared Spectrometer (CIRS) found that the fissures are at least  $-183^\circ\text{C}$ ,  $15^\circ$  warmer than most of the moon's surface.<sup>6,10</sup> Later observations confirmed that the tiger stripe cracks are generally  $60\text{-}80^\circ\text{C}$  warmer than the surrounding polar region.<sup>6,10</sup>

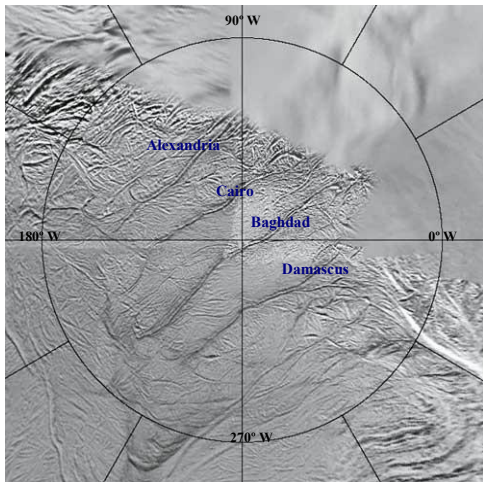


**Fig. 4 Tiger stripes and their given names. Courtesy of NASA JPL, Cassini Outreach.<sup>3</sup>**

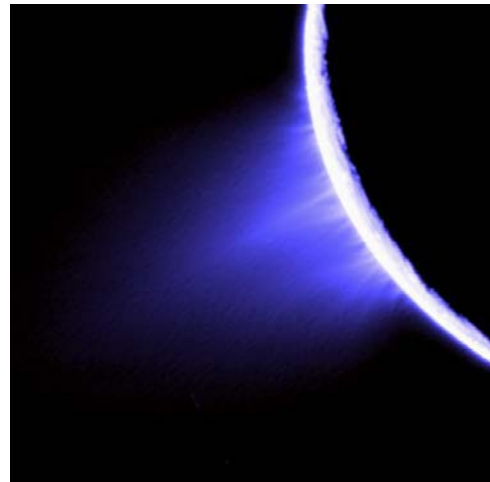


**Fig. 5 Plume emanating from discrete hot spots. Courtesy of NASA JPL, Cassini Outreach.<sup>3</sup>**

The Enceladus plumes consist mostly of water vapor (91%), pouring out at a rate of half a metric ton per second, and other gases including carbon dioxide, nitrogen, methane, ammonia, and possibly other hydrocarbons.<sup>11,12,13</sup> The gas has a scale height of 80 km, according to the Ultra-Violet Imaging Spectrograph (UVIS) team.<sup>9,11</sup> There are also solid particles in the plumes which are probably water ice of typical size 1  $\mu\text{m}$ .<sup>10,14</sup> The particles have a scale height of 30 km, according to the Imaging Science Subsystem team. The larger scale height of the gas implies that the escaping fraction is greater for the gas. Close to the surface, the falloff of density with altitude is much steeper than that of an escaping atmosphere in which both the particles and the gas are moving upward with the thermal velocity of the gas.<sup>14,15</sup> Thus some of the particles are falling back to the surface and some are escaping. Vapor in the plumes escapes at roughly 300 to 500 m/s.<sup>16</sup> However, most of the condensed ice particles fail to reach Enceladus' escape velocity of 240 m/s. New observations confirm that because of the low surface gravity of Enceladus, the plume expands hundreds of kilometers away from the moon, some three times the diameter of the moon, forming a vapor cloud around Saturn which supplies material for Saturn's E-ring. The plume is also the source of neutrals and plasma (neutral OH and atomic oxygen) in Saturn's magnetosphere.<sup>13,14</sup>

Internal heat is most probably the driving factor for Enceladus' plume activity, but how the heat is generated in the interior of the moon is still not clear to scientists. The heat emanating from the south polar terrains (Figs. 6 and 7) has been estimated to be  $5.8 \pm 1.9$  GW.<sup>17</sup> This heat may be coming directly from the core of Enceladus. Cassini has detected dust and ice grains in the plume. This implies that the material must be pulled off of Enceladus with some force, and for this to happen quite a lot of heat is required.<sup>17,18</sup> Scientists believe this amount of heat is way too much to originate from the core of Enceladus.

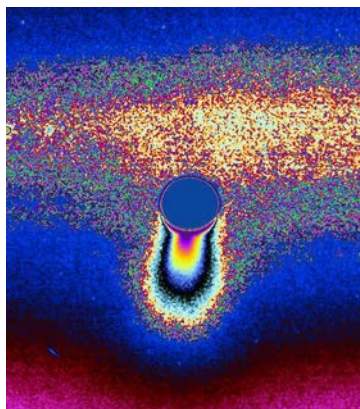


**Fig. 6 Relative height of plume. Courtesy of NASA JPL, Cassini Outreach.<sup>3</sup>**

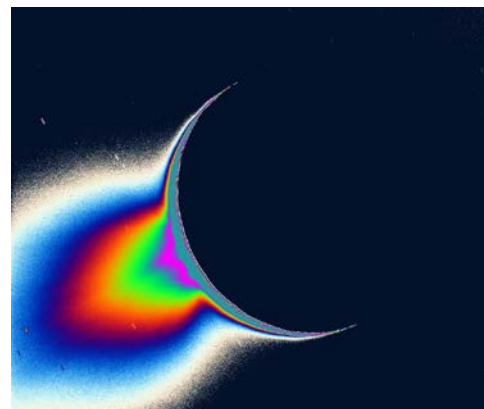


**Fig. 7 Temperature contours of plume coma. Courtesy of NASA JPL, Cassini Outreach.<sup>3</sup>**

The most prevailing explanation for the plume activity has always been that the venting is caused by the tidal forces within the Saturnian system. Saturn's gravity may be squeezing and stretching Enceladus, providing energy which heats up the moon through the process of *tidal frictional heating*.<sup>18,19,20</sup> According to this theory, the surface fractures open and close under Saturn's gravity pull and the Saturn's tides control the timing of the geysers' eruptions causing the flux of jets to vary periodically over a full Enceladus orbit around Saturn.<sup>20,21,22</sup> The proximity of Enceladus to Saturn means that tidal dissipation should have quickly circularized the orbit. A 2:1 mean motion resonance with the moon Dione, which orbits just beyond Tethys, further excites the orbital eccentricity to the observed value of 0.0047, which in turn produces periodic tidal stress on the surface.<sup>18,19</sup> However, the equilibrium tidal heating cannot account for the 5.8 GW heat that is observed to be coming from Enceladus. Some areas on Enceladus' surface, as observed by Cassini scientists, show no craters. This has indicated major geological resurfacing activities in recent past<sup>3</sup> (Fig. 8). Equilibrium heating in possible past resonances cannot explain prior resurfacing events.<sup>18,20</sup>

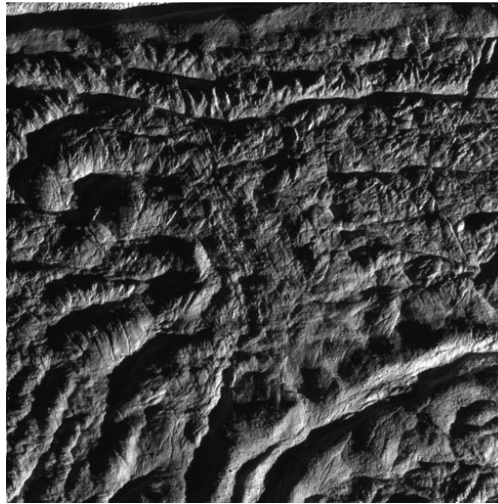


**Fig. 8** The close-up view of Enceladus south polar region, taken on October 31, 2008. No crater is observed in this region. Courtesy of NASA JPL, Cassini Outreach.<sup>3</sup>

Scientists have theorized various models of the Enceladus plumes.<sup>16,17, 23,24</sup> In one model, the water originates in a clathrate reservoir.<sup>17</sup> Clathrate is a material formed by a weak chemical compound consisting of a lattice of one type of molecule trapping and containing a second type of molecule in spaces left by the first. In an alternate model some scientists suggest that the liquid water may exist as close as 7 m to the surface.<sup>17</sup> Both of these suggested models require large amount of energy input to drive the plumes. Anyhow, most of scientists have recently come to the conclusion that there probably is water beneath the surface of Enceladus.<sup>10</sup> Localized subsurface melting on Enceladus may have produced an internal south polar sea and evidence for this localized sea comes from the shape of Enceladus, which does not match a differentiated body at its current orbital position.<sup>10,17</sup>

The south polar jets expel tiny ice grains and vapor, some of which escape the moon's gravity and form Saturn's outermost ring. Cassini's Cosmic Dust Analyzer (CDA) has examined the composition of those grains and found salt within them. Salty minerals deep inside Enceladus are washed out from rock at the bottom of a liquid layer. Liquid water must be present because it is the only way to dissolve the significant amounts of minerals that would account for the levels of salt detected. Scientists now believe that finding salt in the plume gives evidence for liquid water below the surface. Enceladus shows the evidence of ammonia.<sup>11</sup> In space, the presence of ammonia provides strong evidence for the existence of at least some liquid water. Just how much water is contained within Enceladus' icy interior is still not known. At least on Earth, where liquid water and organics exist, there is life. Whether there is life on Enceladus, we don't know yet, but we do know that Enceladus contains potential habitable environments. The presence of liquid water inside Enceladus would have major implications for future astrobiology studies on the possibility of life on bodies in the outer solar system.

## Low-Altitude Cassini Flybys of Enceladus

Determining the nature and origin of the plume material is a top priority for Cassini during its mission. Cassini has executed multiple flybys of Enceladus after arrival at Saturn in June 2004. These flybys have emphasized different science objectives, such as the Ion and Neutral Mass Spectrometer (INMS) observation<sup>11</sup> and radar mapping. Most of these flybys have been at high and very high altitudes, but 5 of them by far are low-altitude flybys with their Enceladus closest approach (ECA) altitudes less than 500 km (Table 1). These 5 flybys are numbered E2, E3, E4, E5, and E6, respectively. The E2 and E3 flybys were executed during Cassini’s prime mission. The Equinox extended mission of Cassini started in July 2008, a month before the E4 flyby.

In order to maintain a stable attitude during the course of Cassini mission, two distinct control systems are used: the attitude controller using the Reaction Control System (RCS) thrusters, and the attitude controller using the reaction wheels.<sup>2</sup> During a low-altitude Enceladus flyby, either reaction wheels or attitude control thrusters on the Cassini spacecraft are used to overcome the external torque imparted on Cassini due to plume and jets, as well as to slew the spacecraft in order to meet the pointing needs of the science instruments. If the imparted torque is larger than it can be handled by the reaction wheel control system, thrusters are used to control the spacecraft during the flyby.

The Cassini spacecraft was under RCS thruster control during only one of the 5 low-altitude flybys (E5) because the AACS had predicted that the external torque imparted on the spacecraft due to the plume and jets during E5 flyby would overwhelm the reaction wheel control. This prediction was done using the engineering model of the Enceladus plume density, as a function of the flyby altitude, and the details of the model will be discussed in the next section. The other 4 low-altitude flybys (E2, E3, E4, and E6) were executed under reaction wheel control. The E5 flyby has been the closest flyby of Enceladus by far with an ECA altitude of 25 km. It has also been among the fastest flybys of Enceladus. The Cassini spacecraft’s flyby speed for E3 was approximately 14.4 km/s and for E4, E5, and E6 17.7 km/s.

**Table 1 Low-altitude Enceladus flybys during Cassini Equinox extended mission**

Enceladus Flyby	Date	Closest Altitude, km	Active Control System
E2	July 14, 2005	175	Reaction Wheel Control
E3	March 12, 2008	50	Reaction Wheel Control
E4	August 11, 2008	50	Reaction Wheel Control
E5 <sup>a</sup>	October 9, 2008	25	RCS Thruster Control
E6	October 31, 2008	196	Reaction Wheel Control

<sup>a</sup>By far the lowest altitude Enceladus flyby.

In 2005, Cassini flew by Enceladus three times at altitudes less than 1300 km. In that same year, Cassini’s UVIS observed stellar occultations on two flybys and confirmed the existence, composition, and the nature of the water vapor plume in the south polar region of Enceladus. UVIS is one of the 12 instruments installed on board Cassini and measures the ultraviolet light in the Saturnian system. Data from UVIS provides information on the atmospheric composition and photochemistry of Saturn and Titan, and the nature and history of Saturn’s rings. On July 14, 2005, Cassini swung by Enceladus at a closest approach altitude of about 175 km and snapped images of the Tiger Stripes. During this flyby, a substantial atmospheric plume and coma were observed, detectable in the INMS data set out to a distance of over 4000 kilometers from Enceladus. Meanwhile, Cassini’s Composite Infrared Spectrometer (CIRS) picked up unexpectedly strong infrared radiation (heat) from the south pole and found that the fissures are at least 90 degrees Kelvin (-183°C), 15° warmer than most of the moon’s surface. Observations by CIRS suggest that the surface temperature along several fractures of the Tiger Stripes was at least 145 K and could have been as high as 180 K.<sup>16</sup>

During Cassini’s E3 closest approach, on 12 March 2008, two instruments were collecting data: the CDA and the INMS. An unexplained software hiccup with Cassini’s CDA instrument prevented it from collecting any data during closest approach, although the instrument did get data before and after the approach. The new data provided a much more detailed look at the fractures that modify the surface and gave a significantly improved comparison between the geologic history of the moon’s north pole and south pole. Cassini flew by Enceladus on August 11, 2008 a mere 50 kilometers from the surface during the E4 flyby. Just after closest approach, all of the spacecraft’s cameras focused on the tiger stripes in order to get more high-resolution images and remote sensing data. “Looking” inside one of the fissures in high

resolution provided more information on the terrain and depth of the fissures, as well as the size and composition of the ice grains inside. Refined temperature data has helped scientists determine if water, in vapor or liquid form, lies close to the surface and better refine their theories on what powers the jets. Imaging sequences captured stereo views of the north polar terrain and high resolution images of the south polar region. Instruments on board Cassini have also helped determine the size of the ice grains and distinguish other elements mixed in with the ice, such as oxygen, hydrogen, or organics.

The E5 flyby took the spacecraft deeper into the south polar plume<sup>3</sup> (Fig. 9). The science priority for this flyby was given to the in situ instruments, which obtained high-resolution data of the plume, which helped the Cassini science team learn more about the composition of both the gaseous and particle components. The last completed low-altitude Enceladus flyby at the time of writing this paper has been the E6 flyby. This flyby was dedicated to remote-sensing. Scientists looked at the south pole of Enceladus for a last time before it headed mostly into seasonal darkness<sup>3</sup> (Fig. 8).

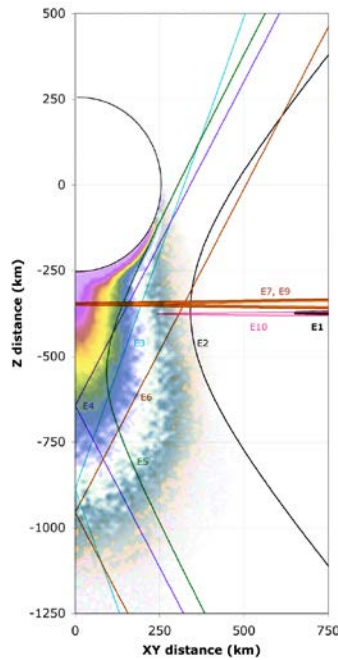


**Fig. 9 Low-altitude Enceladus flybys of Cassini during the prime and Equinox extended missions, courtesy of NASA JPL, Cassini Outreach.<sup>3</sup>**

The remaining three low-altitude Enceladus flybys of Cassini during the Equinox extended mission are summarized in Table 2. The spacecraft will be under RCS thruster control during E7 flyby. For the E9 flyby, the decision of whether thruster control or reaction wheel control will be used is not yet finalized, but the current baseline is RCS thruster control, as indicated in Table 2.

**Table 2 Remaining low-altitude Enceladus flybys of the Cassini Equinox mission**

Enceladus Flybys	Date	Closest Altitude, km	Flyby Speed, km/s	Active Control System
E7	November 2, 2009	100	7.74	RCS Thruster Control
E9	April 28, 2010	100	6.51	RCS Thruster Control
E10	May 18, 2010	439	6.52	Reaction Wheel Control

Cassini Solstice extended mission will officially start on October 1, 2010 and will last for approximately 7 years. A total of 7 low-altitude Enceladus flybys, numbered E12 through E21, with ECA altitudes ranging from 50 km to 100 km are being planned to be executed in this mission, as shown in Table 3, encompassing various science observations of Enceladus plume.

**Table 3 Low-altitude Enceladus flybys during Cassini Solstice extended mission**

Enceladus Flybys	Date	Closest Altitude, km	Flyby Speed, km/s
E12	November 30, 2010	50	6.26
E13	December 21, 2010	50	6.22
E14	October 1, 2011	100	7.43
E17	March 27, 2012	75	7.48
E18	April 14, 2012	75	7.48
E19	May 2, 2012	75	7.51
E21	October 28, 2015	50	8.49

### Enceladus Plume Density Modeling

The main objective of modeling the Enceladus plume density by AACS, as a function of flyby altitude, is to be able to simulate and predict the external torque imparted on Cassini due to the plume and jets during a low-altitude Enceladus flyby, such as E3, E4, etc. The purpose of quantifying such external torque is to analyze its impact on both reaction wheel and thruster control authorities as well as the wheels' spin rate change. The engineering model described in this section is developed, tested, and calibrated by this author for the AACS use. A ground software tool has also been developed by the author to speed up the process of simulating the density of plume and jets, as well as the associated external torque, for any projected low-altitude Enceladus flyby. In order to maintain even better accuracies for future Enceladus flybys, the model has been calibrated after every low-altitude Enceladus flyby.

This engineering model has already been implemented in the Cassini high fidelity test-bed, called the Flight Software Development System (FSDS), as well as the Cassini hardware-in-the-loop integrated testing environment. The FSDS is a high-fidelity test-bed that is used to perform Cassini Guidance and Control (G&C) and Fault Protection (FP) simulations. It is a closed-loop environment using the latest version of the AACS flight software. It has been used extensively by the AACS team to develop and validate AACS flight software loads, perform G&C and FP testing of four critical events for Cassini, i.e. the launch, Saturn orbit insertion, Probe release, and Probe relay tracking. The FSDS is also used to check first-time events, and to investigate flight anomalies. The spacecraft's dynamics model in FSDS includes a rigid body plus system flexibilities such as the Magnetometer boom, the Radio and Plasma Wave Science antennas, and propellant sloshing. This model will be tweaked in future as more density data is collected or reconstructed through upcoming low-altitude Enceladus flybys, such as E7 and E9.

Before starting the discussion of the engineering model, let's first determine the transformation matrix from the Earth-Mean-Equatorial (EME) 2000 inertial frame, also known here as the J2000 frame, to the Enceladus-centric body-fixed coordinates. The ground software tool determines this matrix by first loading the spacecraft position and velocity states in EME-2000 frame for a given Enceladus flyby using the Enceladus and spacecraft ephemerides near the ECA time, specifically in the time interval of  $ECA \pm 30$  min. The states are available in 1-second intervals, and therefore the frequency by which the tool operates is 1 Hz. The tool also loads the Enceladus-Saturn distance ( $d_{ES}$ ) at the time of  $ECA - 30$  min. First, the start time is set up to be  $ECA - 30$  min, and the parameters year ( $Y_S$ ), day of year ( $D_S$ ), hours ( $H_S$ ), minutes ( $M_S$ ), and seconds ( $S_S$ ) are determined using the start time. Then the number of days ( $d$ ) and Julian centuries ( $T$ ) past 12:00 noon of 1/1/2000 epoch are determined using:

$$d = [365.25(Y_S - 2000) + D_S - 0.5] + \frac{360H_S + 60M_S + S_S}{86400} \quad (1)$$

$$T = \frac{d}{36525} \quad (2)$$

The parameter  $T$  is the evaluation time given as an interval since the standard epoch ( $J2000 = JD2451545.0$ ) in Julian centuries of 36525 days each. At this time, the following set of 22 numerical coefficients are identified.<sup>5</sup> These coefficients will be used in subsequent equations. A set of 4 parameters,  $S_1$ ,  $S_2$ ,  $S_3$ , and  $S_4$  are now determined using  $T$ .<sup>5</sup>



where  $R_i$  ( $i = 1, 2, 3$ ) is the rotation matrix about the  $i^{\text{th}}$  axis. The head and tail of the spacecraft position vector in J2000 frame,  $\vec{r}_{J2000}$ , as a function of time are the center of Enceladus and the spacecraft's center of mass, respectively. The spacecraft's range distance, denoted by  $d_{Range}$ , is simply the magnitude of the vector  $\vec{r}_{J2000}$ . This vector is transformed to Enceladus body-fixed coordinates, and the unit vector  $\hat{u}_{SC}$  is constructed using Eq. 12. This unit vector, a function of time, determines the location of Cassini spacecraft in Enceladus frame at any time during ECA  $\pm 30$  min (sampled once every second). The notation  $\|\cdot\|$  denotes the magnitude of a vector.

$$\hat{u}_{SC} = \frac{C_{J2000}^{Enc} \vec{r}_{J2000}}{\|C_{J2000}^{Enc} \vec{r}_{J2000}\|} \quad (12)$$

To model the plume density, a set of eight cones (for plume) and eight cylinders (for jets) are constructed around the eight jet sources on the four major tiger stripes near the Enceladus south polar region. The tiger stripes run for about 130 km across the southern polar region, from  $65^\circ$  S pole-ward, and are about 2 km wide. Table 4 summarizes the locations of these hot spots. The source of this table is Reference 7 (Spitale and Porco). The apex of each cone is assumed to be below the surface of Enceladus at a depth of  $d_{Depth,i}$  ( $= 1$  km), which is a reprogrammable parameter in the ground software tool ( $i = 1, \dots, 8$ ). The plume cones have a half cone angle of  $\beta_{m,i}$  ( $= 45^\circ$ ) with each angle being again a reprogrammable parameter in the ground software tool. The radius of each cylinder associated with a jet is assumed to be  $r_{Jet,i}$  ( $= 1$  km), and all eight radii are reprogrammable as well.

**Table 4 Jet source locations.**

Cone and Cylinder	Sulcus on Tiger Stripes	Latitude, $^\circ$	Longitude, $^\circ$ W
I	Baghdad	-81.5	32.8
II	Damascus	-79.4	315.5
III	Damascus	-81.3	292.8
IV	Alexandria	-72.9	148.7
V	Cairo	-78.6	72.3
VI	Baghdad	-87.1	231.4
VII	Baghdad	-74.6	29.8
VIII	Cairo	-82.1	115.5

Enceladus is modeled as an ellipsoid with tri-axial  $x$ ,  $y$ , and  $z$  dimensions of  $a = 256.6$  km,  $b = 251.4$  km, and  $c = 248.3$  km, respectively. Fig. 11 captures the geometry of one of the eight plume cones in Enceladus coordinates. The point  $Q_i$  is the  $i^{\text{th}}$  plume's center of activity ( $i = 1, \dots, 8$ ) with coordinates of  $(\varphi_i, \theta_i, \lambda_i)$  with  $\varphi_i$  being the latitude,  $\theta_i$  the longitude, and  $\lambda_i$  the distance  $OQ_i$ . The parameters  $\varphi_i$  and  $\theta_i$  are extracted from Table 4 for each cone; however, the longitude  $\theta_i$  is determined after subtracting the longitude listed in the last column of Table 4 from  $360^\circ$ . The parameter  $\lambda_i$  is determined using Eq. 13:

$$\lambda_i = \left\{ \left( \frac{\cos \varphi \cos \theta}{a} \right)^2 + \left( \frac{\cos \varphi \sin \theta}{b} \right)^2 + \left( \frac{\sin \varphi}{c} \right)^2 \right\}^{-\frac{1}{2}} \quad (13)$$

Using the locations of the points  $P_i$  and  $Q_i$  ( $i = 1, \dots, 8$ ) for the eight plume cones, and the unit vector  $\hat{u}_{SC}$  obtained from Eq. 12 along with the spacecraft's range distance ( $d_{Range}$ ), a set of two new unit vectors is defined. The unit vector  $\hat{u}_{Q,i}$  is along the vector connecting the center of Enceladus ( $O$ ) to the  $i^{\text{th}}$  plume's center of activity ( $Q_i$ ), and the unit vector  $\hat{u}_{PS,i}$  is along the vector connecting the  $i^{\text{th}}$  plume's apex point  $P_i$  to spacecraft defined by Eq. 14:

$$\hat{u}_{PS,i} = \frac{d_{Range} \hat{u}_{SC} - (\lambda_i - d_{Depth,i}) \hat{u}_{Q,i}}{\|d_{Range} \hat{u}_{SC} - (\lambda_i - d_{Depth,i}) \hat{u}_{Q,i}\|} \quad (14)$$

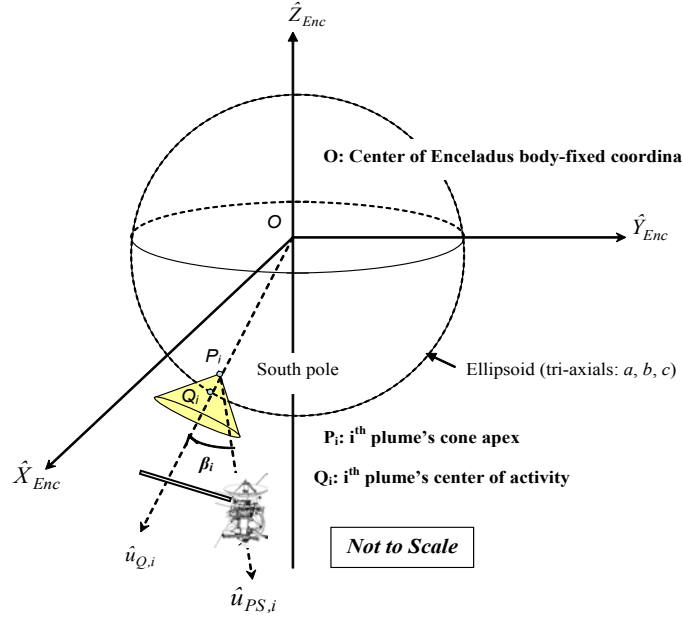


**Fig. 11 Geometry of one of the eight cones**

We proceed with determining another pair of parameters  $d_{QS,i}$  and  $\hat{u}_{QS,i}$  (not shown in Fig.11). The parameter  $d_{QS,i}$  is simply the magnitude of the vector connecting  $Q_i$  to the spacecraft for the  $i^{\text{th}}$  cone, and  $\hat{u}_{QS,i}$  is the unit vector along this vector. The unit vector  $\hat{u}_{SC}$  and the spacecraft's range distance are used to determine the latitude and longitude of the “sub-satellite” trajectory, or surface trajectory of spacecraft, using Eqs. 15 and 16. Then, the spacecraft's flyby altitude from the surface of Enceladus, denoted by  $h$ , is determined using Eq. 17.

$$\varphi_{SS} = \text{Tan}^{-1} \left( \frac{u_{SC}(2)}{u_{SC}(1)} \right) \quad (15)$$

$$\theta_{SS} = \text{Sin}^{-1} [u_{SC}(3)] \quad (16)$$

$$h = d_{Range} - \left\{ \left( \frac{\cos \varphi_{SS} \cos \theta_{SS}}{a} \right)^2 + \left( \frac{\cos \varphi_{SS} \sin \theta_{SS}}{b} \right)^2 + \left( \frac{\sin \varphi_{SS}}{c} \right)^2 \right\}^{-\frac{1}{2}} \quad (17)$$

The inverse tangent function shown in Eq. 15 is equivalent to the “atan2” function in MATLAB, and the parameters  $u_{SC}(1)$ ,  $u_{SC}(2)$ , and  $u_{SC}(3)$  are the X, Y, and Z components of the unit vector  $\hat{u}_{SC}$ . MATLAB is a numerical computing environment and fourth generation programming language developed by The MathWorks.

Finally, the angle made between  $\hat{u}_{PS,i}$  and  $\hat{u}_{QS,i}$  unit vectors for the  $i^{\text{th}}$  cone, denoted by  $\beta_i$  as shown in Fig. 11, is determined by the dot product in Eq. 18. Also, the angle made between  $\hat{u}_{QS,i}$  and  $\hat{u}_{Q,i}$  unit vectors for the  $i^{\text{th}}$  cone, denoted by  $\gamma_i$  (nor shown in Fig. 11), is determined by the dot product in Eq. 19.

$$\beta_i = \text{Cos}^{-1} \left( \hat{u}_{PS,i} \cdot \hat{u}_{Q,i} \right) \quad (18)$$

$$\gamma_i = \text{Cos}^{-1} \left( \hat{u}_{QS,i} \cdot \hat{u}_{Q,i} \right) \quad (19)$$

Fig. 12 shows the eight plume cones and the eight jet cylinders, not drawn to scale. One face of the  $i^{\text{th}}$  cylinder is on the surface of Enceladus, its center is at the point  $Q_i$ , and its radius is  $r_{Jet,i}$  ( $i = 1, \dots, 8$ ).

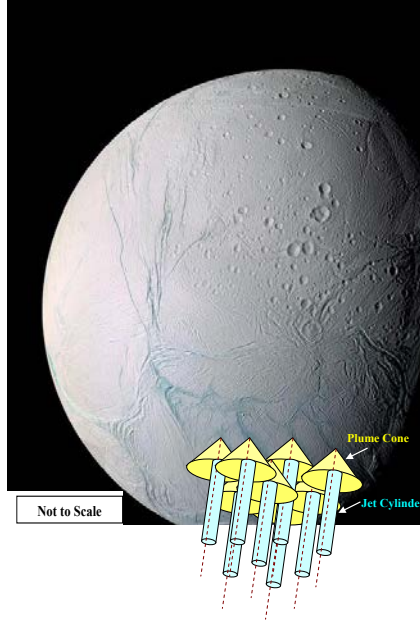


**Fig. 12 Plume and jet models represented by cones and cylinders, respectively.**

The parameters  $\hat{u}_{PS,i}$ ,  $\hat{u}_{QS,i}$ ,  $d_{QS,i}$ ,  $\beta_i$ ,  $\gamma_i$ , for  $i = 1, \dots, 8$ , and  $h$  are all strong functions of time. Throughout the simulation interval of  $ECA \pm 30$  min, for each plume cone and jet cylinder, all these parameters are computed every second. Then,  $\beta_i$  for each cone is compared with  $\beta_{m,i}$ . If  $\beta_i \leq \beta_{m,i}$ , then spacecraft is inside the  $i^{\text{th}}$  cone and the plume mass density for that cone is set to:

$$\rho_i = C_{Coef,i} (h + h_{0,i})^{-2+\varepsilon_i} \quad (20)$$

where  $C_{Coef}$ ,  $h_0$ , and  $\varepsilon$  are  $8 \times 1$  arrays of reprogrammable parameters. The plume and jet density model is calibrated using the peak reconstructed densities for a few past low-altitude flybys of Enceladus, and the best values for  $C_{Coef}$ ,  $h_0$ , and  $\varepsilon$  arrays are determined. Reference 16 has motivated the author to come up with Eq. 20 as discussed later in this section. The current best value of all entries of  $h_0$  array is 20 km, and for the  $\varepsilon$  array, the current best value of all entries is 0.1. Finally, the current best value for all entries of  $C_{Coef}$  array is  $3.911 \times 10^{-8} \text{ kg}\cdot\text{m}^{-3}\cdot\text{km}^{-1.9}$ . Actually, before checking whether the spacecraft is inside the  $i^{\text{th}}$  cone or not, the altitude of the spacecraft is compared with a threshold altitude,  $h_{Thresh}$ , defined as:

$$h_{Thresh} = \min(h_{0,i}) + \left\{ \frac{\rho_{Res}}{\min(C_{Coef,i})} \right\}^{\frac{1}{\varepsilon_i - 2}} \quad (21)$$

where  $\rho_{Res}$  is a reprogrammable parameter currently set to  $10^{-15} \text{ kg}/\text{m}^3$ . This is a “background” density, which is the density of plume 20 Enceladus diameters away, and currently  $h_{Thresh} \approx 9927 \text{ km}$ . If  $h \geq h_{Thresh}$ , then  $\rho_i = \rho_{Res}$ , and  $\rho_i$  is not computed from Eq. 20.

In addition to being inside the  $i^{\text{th}}$  plume cone, in order to check whether the spacecraft is inside the cylinder associated with the  $i^{\text{th}}$  jet, once every second throughout the simulation interval, the angle  $\gamma_i$  is compared with  $\text{Sin}^{-1} \left( \frac{r_{Jet,i}}{d_{QS,i}} \right)$ , and this is done for all jet cylinders. If  $\gamma_i \leq \text{Sin}^{-1} \left( \frac{r_{Jet,i}}{d_{QS,i}} \right)$ , the spacecraft is inside the  $i^{\text{th}}$  cylinder, and the right side of Eq. 20 is multiplied by a reprogrammable parameter known as “jet-to-plume ratio” and denoted by  $k_{JP}$ . The current best value of  $k_{JP}$  based on the results obtained from E5 flyby is 2.3, and  $k_{JP}$  is a single parameter and not an array. Therefore, when inside both the  $i^{\text{th}}$  cone and the  $i^{\text{th}}$  cylinder, the mass density is set to:

$$\rho_i = k_{JP} C_{Coef,i} (h + h_{0,i})^{-2+\varepsilon_i} \quad (22)$$

If  $\beta_i > \beta_{m,i}$ , regardless of the value of  $h$ , the spacecraft is outside the  $i^{\text{th}}$  cone and the plume mass density for that cone is set to  $\rho_{Res}$ .

Reference 18 points out the dependence of eruption activity on the Enceladus-Saturn distance. The tidal forces acting on Enceladus combine with its spin to distort the shape of Enceladus into an ellipsoid whose longest axis points towards Saturn. The rotation rate of Enceladus around its own axis is constant, but the rotational and orbital motions of Enceladus are out of phase. Thus, the line linking Saturn and Enceladus oscillates around a fixed point on the moon's surface, which results in a cyclical "warping" of the shape of Enceladus each day. This constant warping of the moon's surface might be the cause of the stress at the cracks near its southern pole.

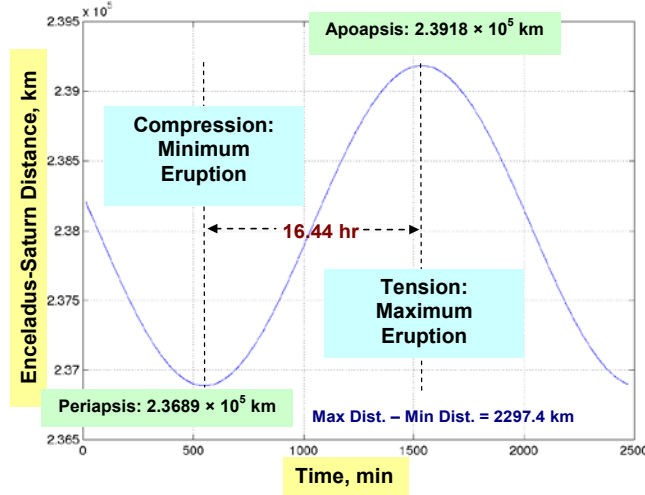


**Fig. 13 Saturn-Enceladus distance variation during on orbital period**

As Enceladus orbits Saturn, the stress changes from compression to tension, allowing the fault to open, possibly exposing liquid water or other volatiles and creating an eruption. The fault remains in tension for half of an orbit, at which point the normal stress once again becomes compressive, forcing the crack to close, ending any possibility of an eruption.<sup>18</sup> Therefore, near periapsis, the cracks are in compression and the eruption activity is minimal (Fig. 13). Near apoapsis, the cracks are in tension and the eruption activity is at its peak.

In the plume density model a set of two reprogrammable parameters are defined. One is the mean distance between Enceladus and Saturn, denoted by  $d_{ES,mean}$  and set equal to 238,035 km, which is the average between the periapsis and apoapsis distances also equal to the semi-major axis of the elliptical orbit of Enceladus around Saturn. The other parameter is  $\Delta_{ES} = 1080$  km, which is a "distance margin" defined for the Enceladus-Saturn mean distance. As mentioned before the ground software tool has the Enceladus-Saturn distance, denoted by  $d_{ES}$ , available at the start time of simulation, i.e. ECA - 30 min. The model has two sets of reprogrammable  $C_{Coef}$  arrays ( $8 \times 1$ ). Set 1 is used for the "high eruption" condition when cracks are in compression and  $d_{ES} \leq d_{ES,mean} + \Delta_{ES}$ . Set 2 is used for the "low eruption" condition when cracks are in tension and  $d_{ES} > d_{ES,mean} + \Delta_{ES}$ . The reprogrammable arrays and parameters used in the model are summarized in Table 5.

**Table 5 Reprogrammable arrays and parameters of the plume density model.**

<b>8 × 1 Arrays</b>	$C_{Coef}$ [set 1], $C_{Coef}$ [set 2], $h_0$ , $\epsilon$ , $d_{Depth}$ , $r_{Jet}$ , $\beta_m$
<b>Single Parameters</b>	$\rho_{Res}$ , $k_{JP}$ , $d_{ES,mean}$ , $\Delta_{ES}$

Reference 16 suggests an expression for the mass density of plume, which is essentially Eq. 23 after some changes in nomenclature.

$$\rho(h) = \rho_0 \left( 1 + \frac{\frac{h}{w}}{1 + \frac{V_h}{V_{th}}} \right)^{-2} \quad (23)$$

where  $\rho_0$  is the plume density at the surface,  $w$  is plume radius on surface ( $\approx 1$  km),  $V_h$  is the particle velocity component perpendicular to the surface, and  $V_{th}$  is the thermal velocity ( $\approx 400$  m/s for water molecules at 180 K).<sup>16</sup> The value of  $V_h$  is typically between 300 to 500 m/s.<sup>16</sup> For typical low-altitude Enceladus flybys with ECA altitudes greater than 25 km,  $h \gg w$  and Eq. 23 basically simplifies to:

$$\rho(h) = \frac{\rho_0}{h^2} \quad (24)$$

However, when  $h$  is zero, Eq. 24 requires  $\rho_0$  to approach infinity, which is unacceptable. In order to avoid this problem, Eq. 24 can be modified to:

$$\rho(h) = \frac{K}{(h + h_l)^2} \quad (25)$$

where  $K$  and  $h_l$  are some general factor and term, respectively. Eq. 25 has motivated the author to come up with Eq. 20. In addition, reference 23 suggests an expression for the modeled mass density of plume, which is Eq. 26 after some changes in nomenclature.

$$\rho(h, \psi) = \rho_0 \left( \frac{R_E}{h + R_E} \right)^2 \exp \left[ - \left( \frac{\psi}{H_\psi} \right)^2 \right] \exp \left[ - \frac{h}{H_d} \right] \quad (26)$$

where  $R_E$  is the mean radius of Enceladus ( $\approx 250$  km),  $\psi$  is the angular distance from the plume center,  $H_\psi$  is the angular width of plume in degrees, and  $H_d$  is a depletion length scale which makes the total gas constant of the plume finite.<sup>23</sup> The parameter  $H_d$  is set equal to 3792 km, and  $H_\psi$  is typically in the range of  $12^\circ$ .<sup>23</sup> With these values for  $H_d$  and  $H_\psi$ , when  $h$  and  $\psi$  are 25 km and  $45^\circ$ , respectively, Eq. 26 is simplified to:

$$\rho(h, \psi) = \frac{C \rho_0 R_E^2}{(h + R_E)^2} \quad (27)$$

where  $C$  is some general. Eq. 27 is also similar to both Eqs. 25 and 20. The modeled plume density for E3 flyby, which is the output of the ground software tool, is captured in Fig. 14.

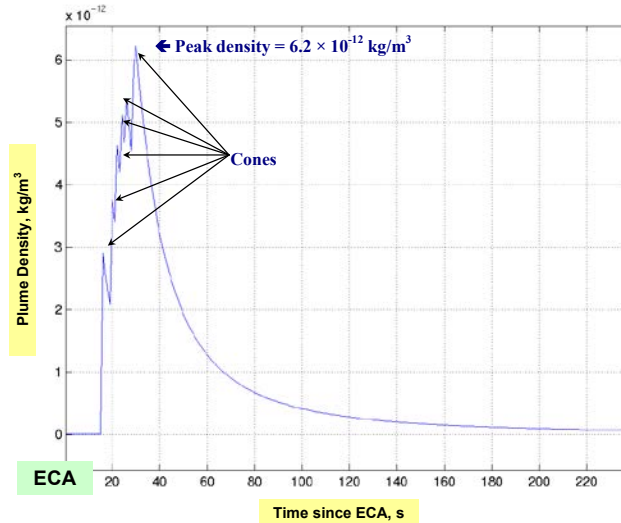


**Fig. 14 Modeled plume density for E3 flyby**

## Reconstruction of Plume Density for a Flyby under Reaction Wheel Control

Cassini has a set of three fixed reaction wheels that are oriented such that their spin axes make equal angles with the spacecraft's Z-axis. Each wheel is considered a Reaction Wheel Assembly (RWA), and the three fixed reaction wheels are named RWA 1, 2, and 3, respectively.<sup>2</sup> In addition, Cassini has a backup, articulatable reaction wheel (RWA 4). Currently, RWA 3 is out of commission and the spin axis of RWA 4 is co-aligned with RWA 3. At Launch, RWA-4 was aligned parallel with RWA-1. On July 11, 2003, the platform was articulated to align the backup reaction wheel with the reaction wheel RWA-3, because the bearings of RWA-3 had developed occasional excessive frictional torque.<sup>2</sup> Each wheel has a wheel spin axis, with one direction designated as the positive spin direction. Location and orientation of Cassini reaction wheels are shown in Fig. 15.<sup>2</sup>

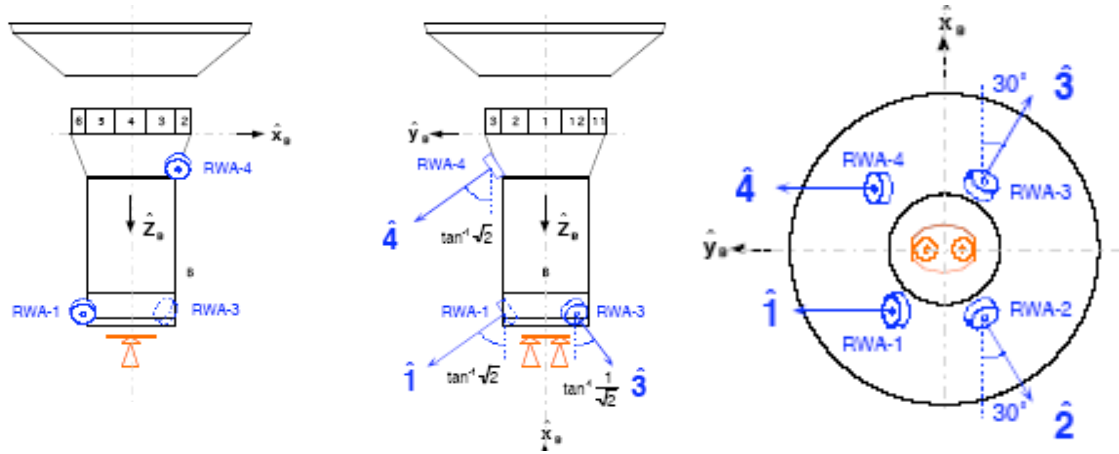


Fig. 15 Locations and orientation of Cassini reaction wheels.

The reaction wheel control system is a proportional-plus-derivative controller. This control system uses an algorithm that determines the desired torque on the spacecraft, and this torque vector is projected along each wheel axis to determine the contribution of each wheel.<sup>2</sup> The result is then negated to determine the commanded torque on each wheel. The torque of the wheel on the spacecraft is equal and opposite to the torque applied to the wheel itself.

The RWAs are used primarily for attitude control when precise and stable pointing of a science instrument is required during an observation. The advantages of using reaction wheels over thrusters are the conservation of hydrazine and the absence of unwanted delta-V imparted on the spacecraft. Typically, Cassini is under reaction wheel control during Enceladus flybys. However, the flyby altitude inside the plume region must be sufficiently high so that the external torque imparted on the spacecraft due to the plume and jets is well within the reaction wheels' control authority. If that is not the case, the flyby will be performed under the RCS thruster control.

While under reaction wheel control, the thruster firings are inhibited, and the RWA spin rate telemetry data are used to estimate the three per-axis torques imparted on the spacecraft due to the Enceladus plume and jets. The angular momenta imparted on the spacecraft due to the plume torque are entirely absorbed by wheels, and the change in RWA spin rates is used to estimate the external torque associated with the plume. Since there is a well-defined relationship between the plume torque imparted on the spacecraft and the Enceladus plume density<sup>1</sup>, the estimated torque can be used to reconstruct the plume density. A ground software tool has been developed by the author to reconstruct the Enceladus plume density for E3, E4, E6, and future flybys under reaction wheel control with sensible peak density. The effectiveness of the approach used in this ground software has also been confirmed via numerous simulations.

In this paper the plume density reconstruction process is explained using the E3 flyby as an example. Similar technique and the same ground software tool are used for plume density reconstruction using the collected guidance, navigation, and control data during other Enceladus flybys under reaction wheel control, such as E4 and E6. This paper partly extends on the methodology reported by this author in

Reference 1, which uses the Cassini guidance, navigation, and control data to reconstruct the Titan atmospheric torque imparted on the spacecraft and the atmospheric density, accordingly.

In order to estimate the Enceladus plume density for a given low-altitude flyby, the external torque imparted on the spacecraft due to the plume and jets must first be estimated. The rotational motion of the spacecraft during an Enceladus flyby is governed by the Euler equation expressed in spacecraft body-fixed coordinate system:<sup>1</sup>

$$I\dot{\vec{\omega}} + \vec{\omega} \times (I\vec{\omega} + \vec{H}_{RWA}) = \vec{T}_{Thruster} + \vec{T}_{RWA} + \vec{T}_{Plume} + \vec{T}_e \quad (28)$$

Since during the flybys under reaction wheel control, the RCS thruster firings are inhibited, the term  $\vec{T}_{Thruster}$  is dropped from the equation. The vector sum of all other external torques on the spacecraft, denoted by  $\vec{T}_e$ , is defined as:<sup>1</sup>

$$\vec{T}_e = \underbrace{\vec{T}_{GG} + \vec{T}_{RTG} + \vec{T}_{Sol} + \vec{T}_{Mag} + \vec{\zeta}}_{\approx 0} \quad (29)$$

The predominant term in  $\vec{T}_e$  is the gravity-gradient torque. The magnitude of gravity-gradient torque is a function of both spacecraft attitude and its distance from the celestial body, in this case the Enceladus. Gravity-gradient torque for low-altitude Enceladus flybys is in the range of m-Nm. The magnitude of gravity-gradient torque is a function of both the spacecrafts attitude and its distance from Enceladus. The per-axis gravity gradient torque for an Enceladus flyby is given by:<sup>1</sup>

$$\left\{ \begin{array}{l} \tau_x^{GG} = \frac{3\mu_{Enceladus}}{R_0^3} (I_{yy} - I_{zz}) (\hat{R}_0 \cdot \hat{e}_y) (\hat{R}_0 \cdot \hat{e}_z) = \frac{3\mu_{Enceladus}}{R_0^3} (I_{yy} - I_{zz}) \cos \theta_y \cos \theta_z \\ \tau_y^{GG} = \frac{3\mu_{Enceladus}}{R_0^3} (I_{zz} - I_{xx}) (\hat{R}_0 \cdot \hat{e}_x) (\hat{R}_0 \cdot \hat{e}_z) = \frac{3\mu_{Enceladus}}{R_0^3} (I_{zz} - I_{xx}) \cos \theta_x \cos \theta_z \\ \tau_z^{GG} = \frac{3\mu_{Enceladus}}{R_0^3} (I_{xx} - I_{yy}) (\hat{R}_0 \cdot \hat{e}_x) (\hat{R}_0 \cdot \hat{e}_y) = \frac{3\mu_{Enceladus}}{R_0^3} (I_{xx} - I_{yy}) \cos \theta_x \cos \theta_y \end{array} \right. \quad (30)$$

Let's assume:

$$\left\{ \begin{array}{l} c_1 = \cos \theta_y \cos \theta_z \\ c_2 = \cos \theta_x \cos \theta_z \\ c_3 = \cos \theta_x \cos \theta_y \end{array} \right. \quad (31)$$

Then,  $\max(c_i)$ ,  $i = 1, 2, 3$  is  $(\cos 45^\circ)^2 = 0.5$ . The worst gravity gradient torque is given by:

$$\tau_{max}^{GG} = \frac{3\mu_{Enceladus}}{2R_0^3} (I_{max} - I_{min}) \quad (32)$$

where  $I_{max}$  and  $I_{min}$  are the maximum and minimum moments of inertia of the spacecraft, respectively. This worst-case gravity gradient torque for E3 flyby (50 km flyby) is no more than only 0.8 m-Nm.

The torque imparted on the spacecraft due to the plume density, denoted by  $\vec{T}_{Plume}$ , is the unknown quantity to be estimated in Eq. 33. This equation is obtained from Eq. 28 after dropping the negligible terms.

$$I\dot{\vec{\omega}} + \vec{\omega} \times (I\vec{\omega} + \vec{H}_{RWA}) = \vec{T}_{RWA} + \vec{T}_{Plume} + \vec{T}_{GG} \quad (33)$$

Integrating and re-arranging this equation yields:

$$\int_0^t \vec{T}_{Plume} d\tau = \int_0^t \left\{ I\dot{\vec{\omega}} + \vec{\omega} \times (I\vec{\omega} + \vec{H}_{RWA}) - \vec{T}_{RWA} \right\} d\tau - \int_0^t \vec{T}_{GG} d\tau \quad (34)$$

All quantities on the right-hand-side of Eq. 34 are available from either telemetry, at a certain allowable sampling rate, or the ground-estimated values of spacecraft parameters. The estimated rate  $\vec{\omega}(t)$  is available via telemetry at a frequency of 0.25 Hz. The RWA spin rate as a function of time for all 3 prime RWAs is available via telemetry from the on-board FSW named the Reaction Wheel Manager at a frequency of 0.25 Hz. The inertia of each RWA is measured accurately before launch, and the spacecraft's inertia tensor and center of mass location are all estimated via ground tools.

The 3-axis angular momenta in RWA frame are transformed to the spacecraft's fixed frame via the transformation matrix given by Eq. 35.<sup>2</sup> In this equation, the first two columns (for RWA-1 and 2) are determined pre-launch, and the last column (for RWA-4) is estimated after the RWA-4 articulation event in 2003.<sup>2</sup>

$$C_{RWA}^{SC} = \begin{bmatrix} 0 & -\frac{1}{\sqrt{2}} & 0.713318 \\ \sqrt{\frac{2}{3}} & -\frac{1}{\sqrt{6}} & -0.402252 \\ \frac{1}{\sqrt{3}} & \frac{1}{\sqrt{3}} & 0.573909 \end{bmatrix} \quad (35)$$

The ground software first determines the accumulated angular momentum vector profile due to the plume torque using Eq. 34. In order to resolve the problem with noisy data, two best components of the angular momentum vector are first optimally curve-fit using the Nelder-Mead multi-dimensional unconstrained nonlinear minimization technique.<sup>1,25</sup> The fit function is then smoothly differentiated to yield the respective components of the external torque imparted on the spacecraft due to plume each as a function of time. The ground software then proceeds to determine the plume density profile as a function of time and the flyby altitude using the knowledge of spacecraft's center of mass, projected area, and the aero-center along with the estimated drag coefficient in a free molecular flow field and the spacecraft's Enceladus-relative range and velocity data.

In order to reconstruct the Enceladus density, as function of altitude, the spacecraft's orbital states, i.e. the Enceladus-relative range and velocity vectors in the Earth-Mean-Equatorial (EME) 2000 inertial frame, are required by the AACS.<sup>1</sup> Before every Enceladus flyby, these spacecraft orbital states are determined by the Cassini navigation team through a converged orbit determination solution. After the actual flyby and when the Deep Space Network radiometric and doppler data are available, these states are slightly adjusted. Per request from the AACS, the navigation team provides these states in one second steps for the time interval of ECA  $\pm$  30 min. The altitude from the surface of the Enceladus, the unit vector along the spacecraft velocity as expressed in the EME-2000 frame, and the magnitude of the spacecraft's velocity relative to Enceladus are determined from these states.

During an Enceladus flyby, the spacecraft is in a low-density free molecular flow field. In low density flows, the plume can no longer be considered as a continuum because the distance between its individual molecules becomes so great that each particle begins to affect the aerodynamic properties of a body. Under these free molecular flow conditions, common aerodynamic relations, like the Euler and Navier-Stokes equations, fail. Instead, aerodynamic properties must be analyzed using the kinetic theory. For free-molecular flow the value of drag coefficient is constant and approximately equal to 2.2. The real value of drag coefficient depends upon the wall temperature and wall roughness.<sup>1</sup> Equations 36 and 37 show the formulas suggested by References 1 and 2 for cylindrical and spherical shaped spacecraft. Based on these equations, the drag coefficient assumed in this paper for Enceladus flybys by Cassini spacecraft is  $2.2 \pm 0.1$ .

$$\text{Cylinder: } C_D = \frac{\sqrt{\pi}}{S} e^{\left(\frac{-S^2}{2}\right)} \left\{ \left(S^2 + \frac{3}{2}\right) I_0\left(\frac{S^2}{2}\right) + \left(S^2 + \frac{1}{2}\right) I_1\left(\frac{S^2}{2}\right) \right\} + \frac{\pi^{\frac{3}{2}}}{4S} \sqrt{\frac{T_{MLI}}{T_{\infty}}} \quad (36)$$

$$\text{Sphere: } C_D = \frac{2}{\sqrt{\pi} S} e^{\left(\frac{-S^2}{2}\right)} \left(1 + \frac{1}{2S^2}\right) + 2\left(1 + \frac{1}{S^2} - \frac{1}{4S^4}\right) \text{erf}(S) + \frac{2\sqrt{\pi}}{3S} \sqrt{\frac{T_{MLI}}{T_{\infty}}} \quad (37)$$

The E3 flyby is the first Enceladus flyby for which the plume density has been both simulated using the AACS-developed engineering model and reconstructed by AACS. The ECA altitude of E3 flyby is 50 km, the spacecraft's flyby speed is 14.4 km/s, and the projected area near ECA is 18.4 m<sup>2</sup>. During this flyby, the RWA-4 has operated inside the undesirable region of  $\pm$ 300 rpm. The operational time duration each wheel spends inside this "low-rpm" region ( $\pm$ 300 rpm) must be minimized. The reason why this is the case is explained in Reference 2. In general, Cassini operation is required to limit the low-rpm dwell time of each wheel to be less than 12,000 hours for the four-year prime mission. The RWA spin rates for E3 flyby are shown in Fig. 16.

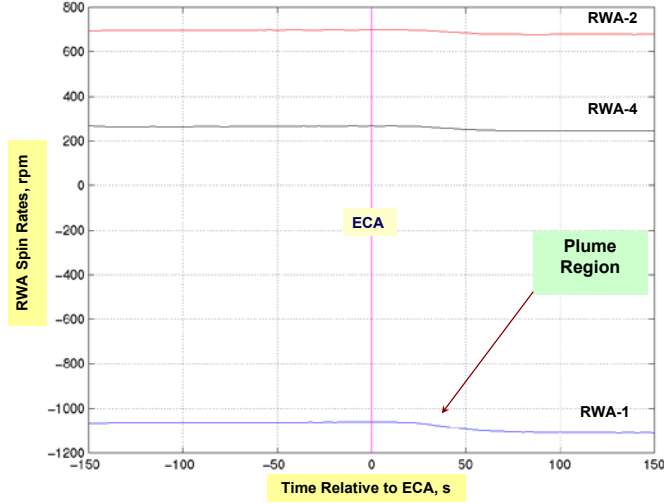


**Fig. 16 RWA spin rate as a function of time relative to ECA for E3 flyby**

The change in RWA spin rates due to external torque of  $\vec{T}_{Plume} + \vec{T}_{GG}$  imparted on the spacecraft is -45 rpm for RWA-1, -18 rpm for RWA-2, and -20 rpm for RWA-4, as shown in Fig. 16. The gravity-gradient torque estimate and its integral are shown in Figs. 17 and 18, respectively.

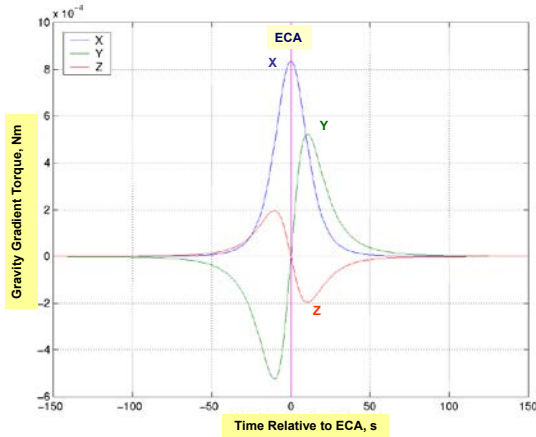


**Fig. 17 Gravity-gradient torque estimate for E3 flyby**

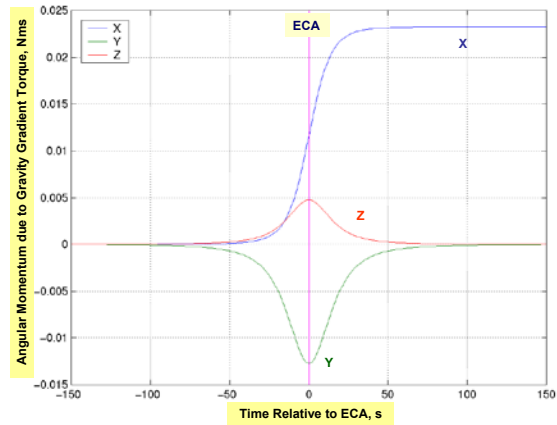


**Fig. 18 Accumulated angular momentum due to the gravity-gradient torque for E3 flyby**

The per-axis accumulated angular momentum in spacecraft fixed body frame due to the plume torque is depicted in Fig 19, and the curve-fit Z-axis angular momentum due to the plume torque is captured in Fig. 20. The fitting function used for the Z-axis fitting during the time interval of  $ECA \pm 150$  s is of the form:

$$H_{Plume,Fit}^Z = -x_1 \{ 1 + \tanh [x_2 (t - t_{ECA} - x_3)] \} + 10^{-4} x_4 t \quad (38)$$

For the smoothed-out Z-axis accumulated angular momentum:  $\vec{X} = [0.4530, 0.0494, 43.2279, 6.2805]^T$ .

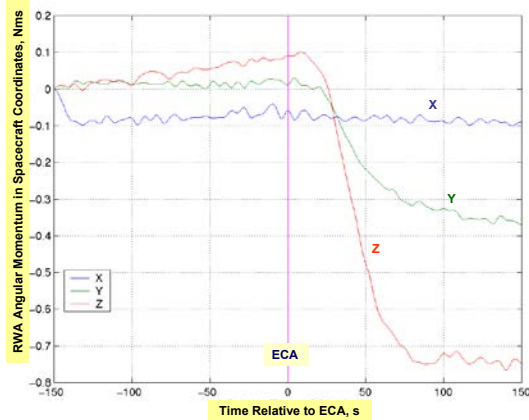


**Fig. 19** Accumulated angular momentum in spacecraft body frame due to the plume torque for E3

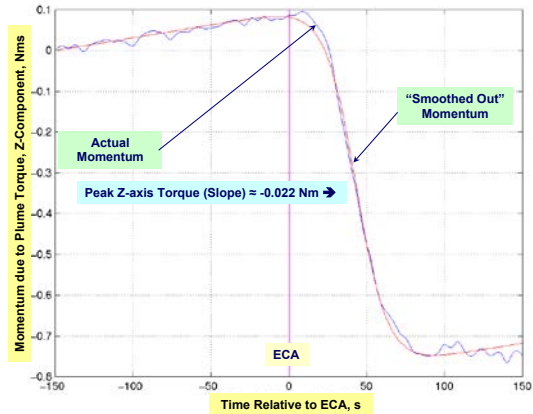


**Fig. 20** Smoothed-out Z-axis angular momentum due to plume torque for E3 flyby

The reconstructed Z-axis plume torque as a function of time relative to ECA and flyby altitude is shown in Figs. 21 and 22, respectively. The peak external Z-axis torque due the plume is  $-0.022$  Nm for E3 flyby and occurs at an altitude of 450 km. Figs. 23 and 24 show the reconstructed plume density for E3 as a function of time since ECA and the flyby altitude, respectively. The reconstructed peak plume density for E3 is  $5.8 \times 10^{-12}$  kg/m<sup>3</sup> and occurs at the same altitude of 450 km.

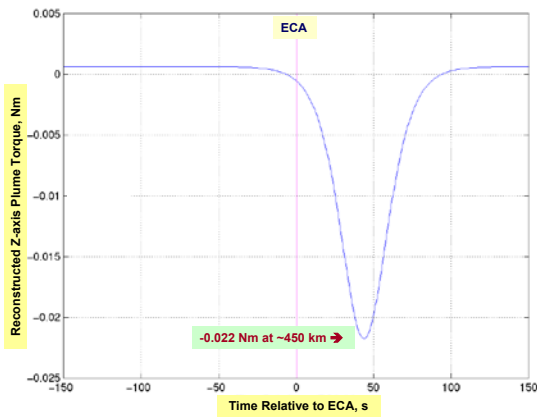


**Fig. 21** Reconstructed Z-axis plume torque as a function of time relative to ECA for E3 flyby

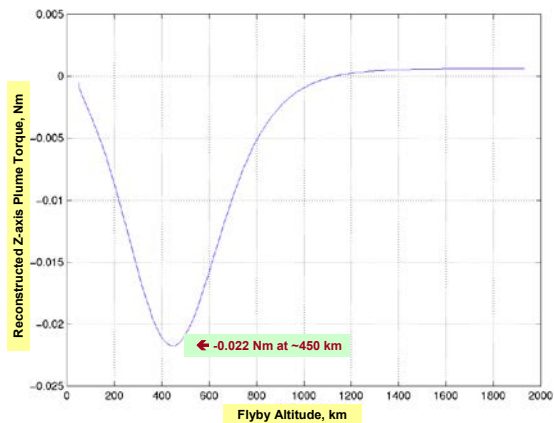


**Fig. 22** Reconstructed Z-axis plume torque as a function of altitude for E3 flyby

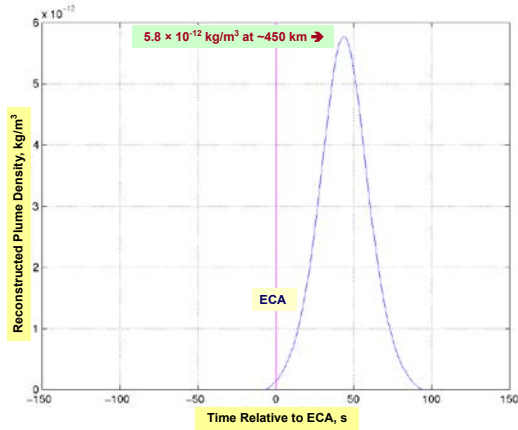


**Fig. 23 Reconstructed plume density versus time since ECA for E3 flyby**

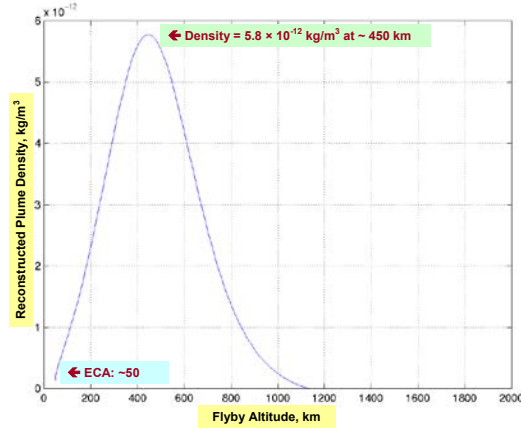


**Fig. 24 Reconstructed plume density as a function of flyby altitude for E3 flyby**

### Reconstruction of Plume Density for an Enceladus Flyby under Thruster Control

The Cassini spacecraft was under RCS thruster control during the 25-km E5 flyby on October 9, 2008. This flyby was the first low-altitude Enceladus flyby on thrusters, and by far the only one. The next low-altitude flyby (E7) on November 2, 2009 is also planned to be executed under RCS thruster control.

The attitude controller using thrusters is a bang-off-bang control system. The RCS system consists of sixteen (eight primary or A-branch and eight backup or B-branch) hydrazine thrusters, placed in four clusters, with a thrust range of 0.5-1.0 N.<sup>26,27</sup> A diagram of thruster locations and thrust directions is depicted in Fig. 25. Pointing control about the spacecraft's X and Y axes are performed using four Z-facing thrusters, while control about the Z-axis is performed using four Y-facing thrusters.<sup>7,8</sup>

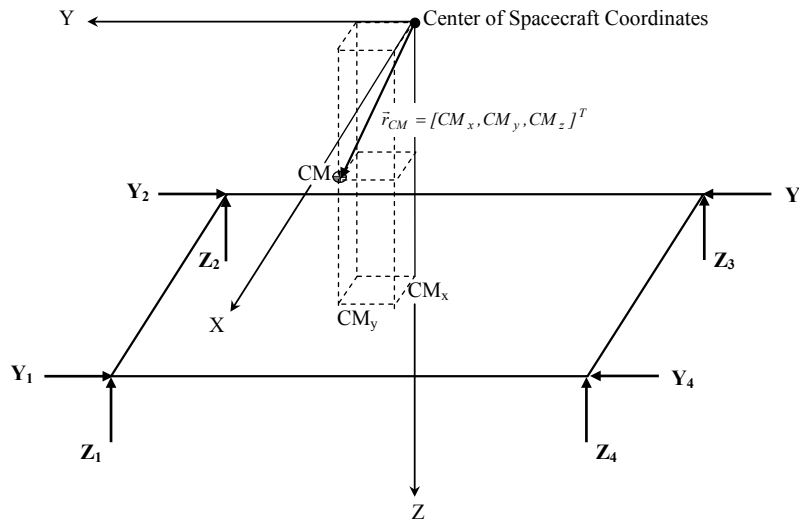


**Fig. 25 Cassini RCS thruster configuration.**

The Monopropellant Tank Assembly (MTA) of Cassini was recharged on April 10, 2006, and this caused an increase of approximately 50% in thrust magnitudes of the primary and backup RCS thrusters. The RCS thruster pulse is modeled according to Fig. 26, which is not drawn to scale. The four parameters  $F_0$ ,  $\Delta$ ,  $t_R$ , and  $t_T$  are the steady-state thrust, the commanded pulse width, the exponential rise-time constant, and the exponential tail-off time constant, respectively. The impulse generated by an “ideal” thruster (with zero rise and tail-off time constants) is highlighted and shown by the dashed line in the figure. The solid thick line indicates the actual pulse. Typical values for  $t_R$  and  $t_T$  are 20 ms and 43-65 ms, respectively. The

rise time remains constant, while the tail-off time varies with time. The tail-off time was about 65 ms before the MTA recharge on April 10, 2006. It dropped to 43 ms after the recharge.

The commanded impulse associated with one single thruster pulse (shaded area) is  $F_0\Delta$ , where  $\Delta$  is the commanded thruster pulse width. The residual impulse ( $I_{res}$ ) is simply the difference between the area under the curve of the actual pulse and that of the ideal pulse.<sup>1</sup> It is equal to:

$$I_{res}(\Delta) = \left( \int_0^{\Delta} F_0 (1 - e^{-t/t_R}) dt + \int_{\Delta}^{\infty} F_0 (1 - e^{-\Delta/t_R}) e^{-(t-\Delta)/t_T} dt \right) - F_0 \Delta = F_0 (t_T - t_R) (1 - e^{-\Delta/t_R}) \quad (39)$$

The residual impulses are accounted for when computing the accumulated angular momentum resulting from RCS thruster firings in a low-altitude Enceladus flyby.

On March 12, 2009, Cassini successfully swapped to the backup RCS thrusters. Shortly after the swap, the nominal operation of the B-branch RCS thrusters was verified by Cassini Attitude and Articulation Control Subsystem (AACCS) team, and the thrust magnitudes of the B-branch thrusters were reconstructed by the author using the telemetry collected during a set of reaction wheel biases and RCS-based slews. Once again, the rise time constant remained unchanged after the swap, but the tail-off time constant was shortened. Not accounting for the larger thrust magnitude of B-branch thrusters compared to A-branch, the X-axis control authority with B-branch thrusters is approximately 4% larger than that generated by A-branch thrusters while the Y and Z-axis control authorities are identical.

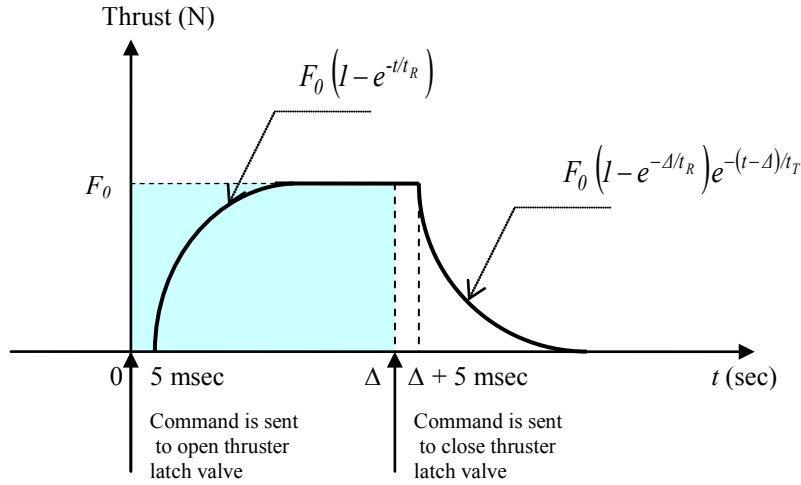


**Fig. 26 The model for an RCS thruster Pulse.**

No Enceladus flyby has been executed using the B-branch thrusters. The 100-km E7 flyby will be the first Enceladus flyby under RCS thruster control using the B-branch thrusters. The thruster firing telemetry data is used to estimate the three per-axis torques imparted on the spacecraft due to the Enceladus plume. Since there is a well-defined relationship between the plume torque imparted on the spacecraft and the plume density, the estimated torque can be used to reconstruct the plume density. The technique used here is very similar to the one used by this author, as described in details in Reference 1, to reconstruct the Titan atmospheric torque imparted on the spacecraft and the atmospheric density. The author has also created special purpose ground software tools to automate the implementation of this methodology, and the effectiveness of this approach has been confirmed via numerous simulations and has been applied on data collected from E5 flyby.

The rotational motion of the spacecraft during the Enceladus flyby is governed by Eq. 28. Both  $\vec{H}_{RWA}$  and  $\vec{T}_{RWA}$  are zero and are dropped out from Eq. 28. This is because at least half an hour before ECA, a transition is made from reaction wheel control to RCS control. All the wheel rates are zero while the spacecraft is under the influence of plume. The torque imparted on the spacecraft due to the plume density, denoted by  $\vec{T}_{Plume}$ , is the unknown quantity to be estimated in Eq. 40. This equation is obtained from Eq. 28 after dropping the negligible terms.

$$I\dot{\vec{\omega}} + \vec{\omega} \times I\vec{\omega} = \vec{T}_{Thruster} + \vec{T}_{Plume} \quad (40)$$

It should also be noted that torque exerted on the spacecraft due to thruster firings,  $\vec{T}_{Thruster}$ , is not available directly from the flight software and should be reconstructed. Integrating Eq. 40 and solving for the accumulated angular momentum due only to plume torque yields:

$$\int_0^t \vec{T}_{Plume} d\tau = \int_0^t \left( I\dot{\vec{\omega}} + \vec{\omega} \times I\vec{\omega} - \vec{T}_{Thruster} \right) d\tau = I[\vec{\omega}(t) - \vec{\omega}(0)] + \int_0^t \vec{\omega} \times I\vec{\omega} d\tau - \int_0^t \vec{T}_{Thruster} d\tau \quad (41)$$

All quantities on the right-hand-side of this equation are available again from either telemetry or ground-estimated values of spacecraft parameters. The accumulated on-times for the eight primary RCS thrusters are available via telemetry from the on-board Propulsion Manager, and the spacecraft's inertia tensor and center of mass location are estimated via ground tools. To resolve the issue of dealing with noisy accumulated angular momentum vector due to the plume torque, the key components of this vector (as functions of time) are "curve-fit" to a sum of two hyperbolic tangent functions of time, using the Nelder-Mead multi-dimensional unconstrained nonlinear minimization technique.<sup>25</sup> The fit function is then smoothly differentiated to yield the respective components of the atmospheric torque vector.<sup>1</sup>

The plume density is related to the torque imparted on the spacecraft. The density (as a function of altitude) is determined using:<sup>1</sup>

$$\vec{T}_{Plume} = \frac{1}{2} C_D \rho V^2 A_{Proj} \hat{u}_V \times (\vec{r}_{CP} - \vec{r}_{CM}) \quad (42)$$

where  $\rho$  is the plume mass density in  $\text{kg/m}^3$ , which is a function of time. The plume density is also a strong function of the flyby altitude. Only one axis of the external torque is essentially required to determine the density from Eq. 42. However, in order to minimize the effect of the slight error in the knowledge of the spacecraft's aero-center (center of pressure) location, two best components of the plume torque vector, e.g. Y and Z, are used to determine the density. The weighted average of the two density profiles, computed from the selected torque components, is determined based on their respective least-squares fit error.<sup>1</sup> The  $3\sigma$  uncertainties in estimated plume torque and density using this technique are better than 12% and 15%, respectively.<sup>1</sup>

The ECA altitude of E5 flyby is 25 km, the spacecraft's flyby speed is 17.7 km/s, and the projected area near ECA is  $18.4 \text{ m}^2$ . Fig. 27 depicts the curve-fit Z component of the accumulated angular momentum due to atmospheric torque for E5 flyby. The fitting function used for both components during the time interval of  $\text{ECA} \pm 15$  minutes is of the form:<sup>1</sup>

$$H_{Plume,Fit}^Z = -x_1 \left( 1 + \tanh \left\{ 10^{-2} x_2 \left( t - t_{ECA} - \delta + 10^2 x_3 \right) \right\} \right) - 10^{-6} x_4 t + 10^{-2} x_5 \tanh \left[ 10^{-2} x_6 \left( t - t_{ECA} - \delta \right) \right] \quad (43)$$

where  $\vec{X} = [x_1, x_2, x_3, x_4, x_5, x_6]^T$  is the coefficient vector for fitting function. For the smoothed-out Z-axis accumulated angular momentum:  $\vec{X} = [1.0523, 5.8668, 1.0167, 7.0875, 5.7031, 2.0107]^T$ , and the total Z-axis accumulated angular momentum during the time interval of  $\text{ECA} \pm 15$  min. is -2.17 Nms. The reconstructed Z-axis plume torque as a function of time relative to ECA is shown in Figs. 28 and 29. The peak external Z-axis torque due the plume is -0.071 Nm for E5 flyby and occurs at an altitude of 185 km. Figs. 30 and 31 show the reconstructed plume density for E5 as a function of time since ECA and the flyby altitude, respectively. The reconstructed peak plume density for E5 is  $1.25 \times 10^{-11} \text{ kg/m}^3$  and occurs at the same altitude of 185 km.

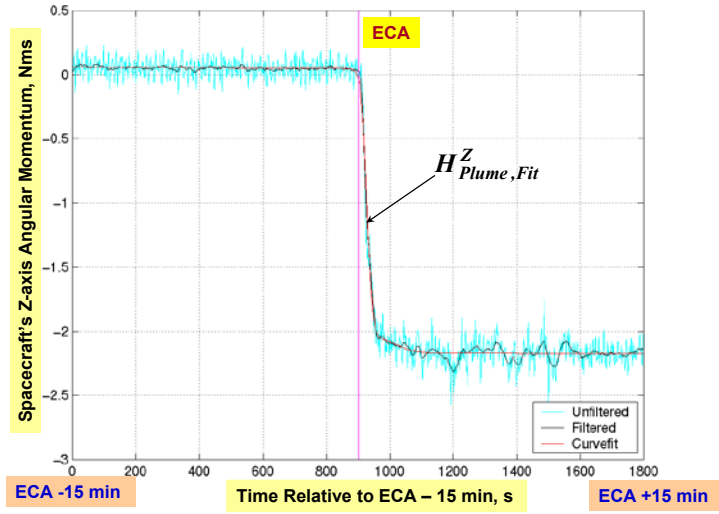


Fig. 27 Spacecraft's Z-axis angular momentum for E5 flyby

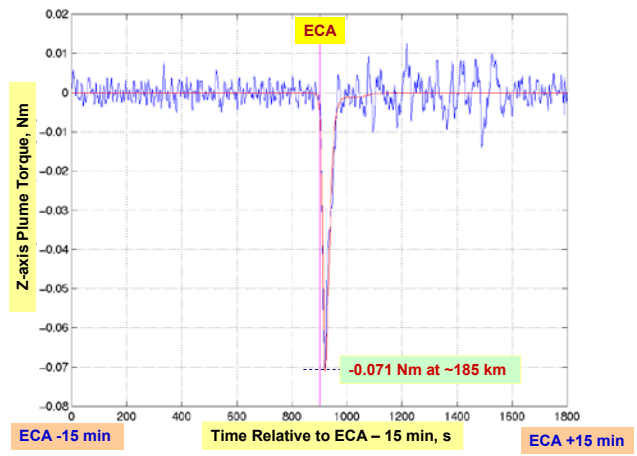


Fig. 28 Z-axis reconstructed plume torque for E5 flyby

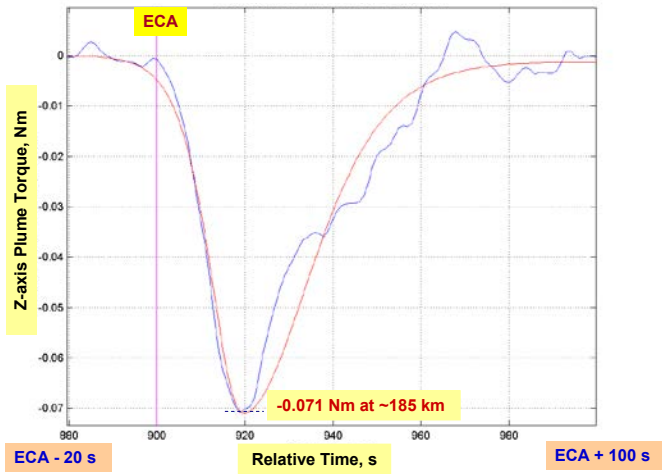
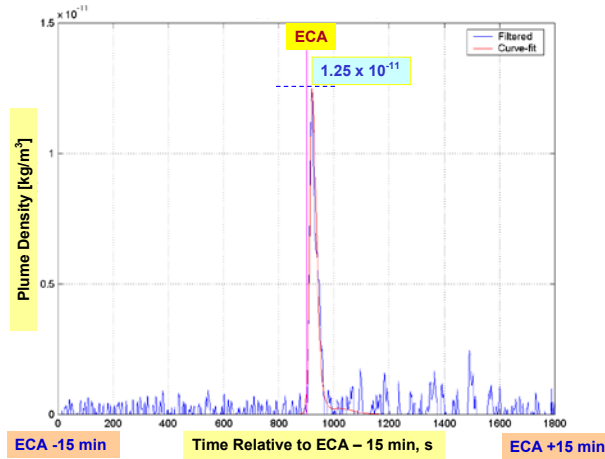
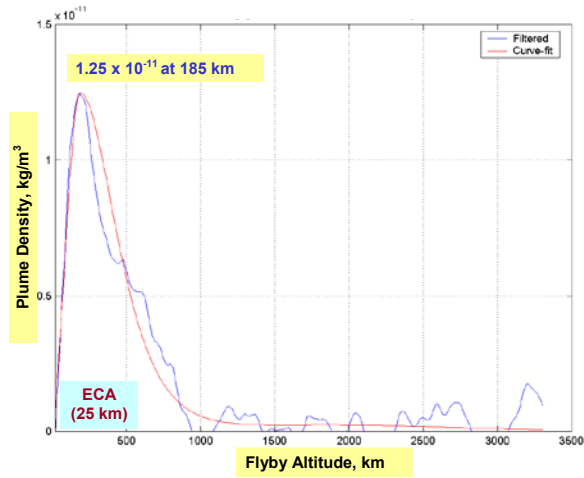


Fig. 29 The “zoomed-in” Z-axis plume torque for E5 flyby



**Fig. 30 Reconstructed plume density for E5 flyby**



**Fig. 31 The “zoomed-in” reconstructed plume density for E5 flyby**

The Cassini AACS flight software has an error monitor called the “filtered disturbance slope high water mark.” This error monitor, which runs once every 125 ms, is originally designed to diagnose a leaky thruster on board the spacecraft, which leads to the excessive thruster commanding. During a low-altitude Enceladus flyby, this error monitor is used to determine the external torque imparted on the spacecraft. In this error monitor, the per-axis time derivative of the accumulated angular momentum vector due to the external torque imparted on the spacecraft is implemented via a lead-lag filter to minimize the error associated with the differentiation of noisy signals,<sup>1,2</sup> and results are available as telemetry data. A set of three AACS telemetry, associated with the filtered disturbance slope high water mark, represents the estimates of the per-axis external torque (in this case the torque due to plume and jets) imparted on the spacecraft. During the E5 flyby the Z-axis filtered disturbance slope high water mark has been -0.163 Nm, while the reconstructed peak Z-axis torque due the plume is -0.071 Nm. The ratio of the two is 2.3. This discrepancy is due the effect of jets. When passing over a narrow jet with a high speed, in excess of 17.7 km/s, the external torque acts like an impulse and for a very short period of time (less than 1 s). Such impulse cannot be reconstructed using the methodology described in this paper, but its effect is modeled in the engineering density model through the parameter  $k_{JP}$ . The value of  $k_{JP}$  in the density model is 2.3. The peak duty cycle of Y2-Y4 thruster pair during E5 flyby is 12%, as shown in Fig. 32.

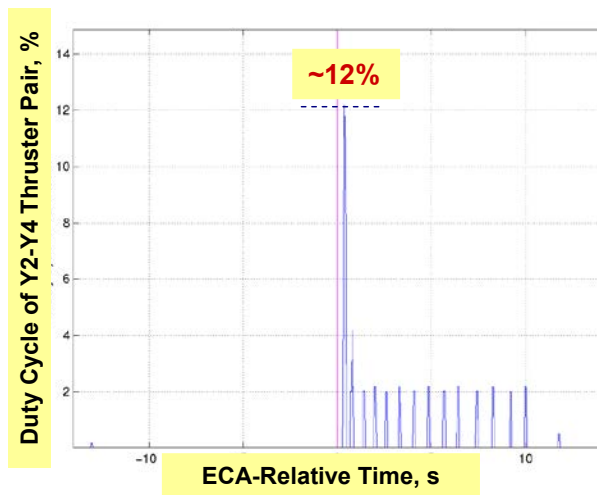


Fig. 32 Peak duty cycle of Y2-Y4 thruster pair during E5 flyby.

### Summary and Conclusions

Cassini continues its successful mission conducting scientific investigations of Saturn and its rings and satellites, including the mysterious Enceladus. Cassini's four-year prime mission has ended in 2008, but this fantastic and sophisticated spacecraft is extending its mission by 9 years and is about to complete its Equinox extended mission. The Enceladus is an active moon of Saturn having water geysers spewing from its tiger stripes, a set of surface cracks near the moon's south pole. By far, the most plausible conjecture that explains this activity is the tidal frictional or shear heating mechanism. According to this conjecture, the tidal forces acting on fault lines in the moon's icy shell cause the sides of the faults to rub back and forth against each other, producing enough heat to transform some of the ice into plumes of water vapor and ice crystals.

Enceladus plume density is not only important to the science community but is particularly important to the Cassini spacecraft operations engineers. Unexpectedly large density profile, and the respective large external torque profile, could potentially cause the spacecraft to tumble out of control during a low-altitude Enceladus flyby. Hence, an accurate estimate of density profile as a function of altitude is required to allow mission planners to select safe flyby altitudes and to allow navigation engineers to accurately predict the delta-V associated with those flybys that are under thruster control.

The described engineering model, and the associated ground software tool, has been developed by the author for the Cassini Attitude and Articulation Control Subsystem that is able to predict and simulate with sufficient accuracy the density of Enceladus plume and jets and the external torque imparted on Cassini spacecraft due to the plume density during all projected low-altitude Enceladus flybys. This model has already been implemented in the Cassini high fidelity test-bed, the Flight Software Development System, as well as the Cassini hardware-in-the-loop integrated testing environment. The peak densities predicted by this model and the reconstructed plume densities of the four low-altitude Enceladus flybys of 2008 have matched closely. In order to maintain even better accuracies for future flybys, the model has been calibrated after every low-altitude Enceladus flyby and has the capability of being tweaked further as more density data is collected or reconstructed.

The novel methodologies reported in this paper are used to reconstruct the Enceladus plume (and jets) density as a function of flyby altitude using Cassini's guidance, navigation, and control data. The effectiveness of these techniques has been demonstrated in four past low-altitude flybys of Enceladus in 2008, under both thruster and reaction wheel control, and will continue to be used on all remaining low-altitude Enceladus flybys in Cassini's extended missions. Density estimates collected from these low-altitude flybys have provided and will continue to provide planetary scientists with valuable data to better understand the plume density structure of Enceladus. These techniques could potentially be modified to reconstruct the atmospheric or plume density of other planets and moons.

## Acknowledgements

The work described in this paper was carried out by Jet Propulsion Laboratory, California Institute of Technology, under a contract with the National Aeronautics and Space Administration. Reference to any specific commercial product, process, or service by trade name, trademark, manufacturer or otherwise, does not constitute or imply its endorsement by the United States Government or the Jet Propulsion Laboratory, California Institute of Technology. The methodologies and the ground software tools described in this paper have been reported to the Patent Counsel Office of Jet Propulsion Laboratory for patent application. The author is indebted to Professor Larry W. Esposito of University of Colorado, Boulder and Dr. Allan Y. Lee, the Project Element Manager of the Cassini Attitude and Articulation Control Subsystem team, for their expert discussions and critiques. The inputs and helpful suggestions from my Navigation, AACS Uplink, Downlink, Propulsion, and Mission Planning colleagues, as well as the Cassini scientists are greatly appreciated. The author is also grateful to Cassini management for its guidance and support. Additional thanks go to Sima Lisman, the Guidance and Control Systems Engineering Group Supervisor, and Dr. Allan Lee for improving on the technical accuracy of this paper through their careful proofreading. Any remaining factual or interpretation errors are of course the author's own responsibility.

## References

- <sup>1</sup>Sarani, S., "A Novel Methodology for Reconstruction of Titan Atmospheric Density Using Cassini Guidance, Navigation, and Control Data," *Proceedings of the AIAA Guidance, Navigation, and Control Conference*, Hilton Head, South Carolina, August 20–23, 2007.
- <sup>2</sup>Lee, A. Y. and Hanover, G. "Cassini Spacecraft Attitude Control System Flight Performance," *Proceedings of the AIAA Guidance, Navigation, and Control Conference*, San Francisco, California, August 15-18, 2005.
- <sup>3</sup>Alice Wessen, "Cassini Equinox Mission" [online database], Cassini Outreach, <http://saturn.jpl.nasa.gov/photos/> [retrieved 1 March 2009].
- <sup>4</sup>Thomas, P.C., et al., "Shapes of the Saturnian Icy Satellites and Their Significance," *Icarus*, April 2007.
- <sup>5</sup>Jacobson, R.A., "The Orientations of the Saturnian Satellites," Jet Propulsion Laboratory, Pasadena, October 2007.
- <sup>6</sup>Matson, D. L., et al., "Enceladus' plume: Compositional evidence for a hot interior," *Icarus*, Vol. 187, October 2006.
- <sup>7</sup>Spitale, J.N. and Porco, C.C., "Association of the Jets of Enceladus with the Warmest Regions on Its South-Polar Fractures," *Nature*, Vol. 449, October 2007.
- <sup>8</sup>Hansen, C. J., et al., "Enceladus' Water Vapor Plume," *Science*, Vol. 311, March 2006.
- <sup>9</sup>Hansen, C. J., et al., "Water vapour jets inside the plume of gas leaving Enceladus," *Nature*, Vol. 456, November 2008.
- <sup>10</sup>Collins, G.C. and Goodman, J.C., "Enceladus's South Polar Sea," *Icarus*, January 2007.
- <sup>11</sup>Waite, J. H., et al., "Cassini Ion and Neutral Mass Spectrometer: Enceladus Plume Composition and Structure," *Science*, Vol. 311, March 2006.
- <sup>12</sup>Hodyss, R., et al., "Release of N<sub>2</sub>, CH<sub>4</sub>, CO<sub>2</sub>, and H<sub>2</sub>O from surface ices on Enceladus," *Icarus*, Vol. 197, March 2008.
- <sup>13</sup>Brown, R. H., et al., "Composition and Physical Properties of Enceladus' Surface," *Science*, Vol. 311, March 2006.
- <sup>14</sup>Hodyss, R., et al., "Photochemistry of methane–water ices," *Icarus*, Vol. 200, October 2008.
- <sup>15</sup>Hedman, M. M., et al., "Spectral Observations of the Enceladus Plume with Cassini-VIMS," *The Astrophysical Journal*, Vol. 693, March 2009.
- <sup>16</sup>Tian, F., et al., "Monte Carlo Simulations of the Water Vapor Plumes on Enceladus," *Icarus*, November 2006.
- <sup>17</sup>Kieffer, S.W., et al., "A Clathrate Reservoir Hypothesis for Enceladus' South Polar Plume," *Science*, Vol. 314, December 2006.
- <sup>18</sup>Hurford, T.A., et al., "Eruptions Arising from Tidally Controlled Periodic Openings of Rifts on Enceladus," *Nature*, Vol. 447, May 2007.
- <sup>19</sup>Dombard, A. J., "Cracks under Stress," *Nature*, Vol. 447, May 2007.
- <sup>20</sup>Nimmo, F., et al., "Shear heating as the origin of the plumes and heat flux on Enceladus," *Nature*, Vol. 447, May 2007.

- <sup>21</sup>Meyer, J. and Wisdom, J., "Tidal Heating in Enceladus," *Icarus*, Vol. 188, March 2007, pp. 535-539.
- <sup>22</sup>Smith-Konter, B. and Pappalardo, R. T. "Tidally driven stress accumulation and shear failure of Enceladus's tiger stripes," *Icarus*, Vol. 198, August 2008.
- <sup>23</sup>Saur, J., et al., "Evidence for temporal variability of Enceladus' gas jets: Modeling of Cassini observations," *Geophysical Research Letters*, Vol.35, October 2008.
- <sup>24</sup>Ingersoll, A. P., et al., "Models of the Enceladus Plumes," *Bulletin of the American Astronomical Society*, Vol. 38, 2006.
- <sup>25</sup>Nelder, J. A. and Mead, R. A., "Simplex Method for Function Minimization," *Computer Journal*, Vol. 7, No. 4, 1965, pp. 308-313.
- <sup>26</sup>Sarani, S., "Assessment of Per-Axis Thruster Control Authority of Cassini Spacecraft for Low Altitude Titan Flybys," Paper AAS 04-275, *14<sup>th</sup> AAS/AIAA Space Flight Mechanics Conference*, Maui, Hawaii, February 8-12, 2004, pp. 4-6.
- <sup>27</sup>Barber, T.J. and Cowley, R.T., "Initial Cassini Propulsion System In-Flight Characterization," AIAA-2002-4152. *38th AIAA/ASME/SAE/ASEE Joint Propulsion Conference and Exhibit*, Indianapolis, Indiana, 2002.